Chapter 5

Objective 2

Amphiphilic Chitosan-based Redox-responsive Nanoparticles for Targeted Delivery of Cabazitaxel to Tumor microenvironment

5 Cabazitaxel-loaded redox-responsive nanocarrier based on D-alpha-tocopheryl-chitosan and hyaluronic acid for improved anti-tumor efficacy in DMBA-induced breast cancer model

5.1 Introduction

Breast cancer is the most prevalent type of cancer accounting for over 25 percent of total cancer cases worldwide. According to GLOBOCAN 2020, there were an estimated 2.3 million new cases of breast cancer globally in 2020 with approximately 685,000 deaths in the same year. The age-standardized mortality rate for breast cancer reported to be 13.0 per 100,000 women and an estimated 5-year prevalence of breast cancer (both sexes, all ages) of around 7.8 million cases [147]. This makes breast cancer a significant health concern and underscores the importance of ongoing efforts in the research to understand its prevalence and the development of effective treatment strategies. Radiation therapy and chemotherapy are the traditional therapeutic strategies in case the surgical removal is not feasible. However, poor clinical results, toxic effects, and drug resistance are the major limitations of traditional treatment strategies.

Nanoparticles have shown great promise in ameliorating the limitations associated with traditional treatment strategies for breast cancer [148,149]. It can utilize the EPR effect to enter the tumor cells [150]. Their submicron size improves cellular uptake and facilitates intracellular delivery of therapeutic agents [151,152]. To improve the selectivity, the surface of nanoparticles can be functionalized with specific ligands [153,154], to ensure precise intracellular delivery of therapeutics via. receptor mediated endocytosis [155,156]. To further improve the precise delivery of therapeutics at target site, nanoparticles responsive to physiological stimuli can be designed [157–160]. Recently, redox responsive nanosystems have gained enormous attention. It releases its payload selectively in the presence of elevated level of reducing agents like glutathione (GSH) in cancer cells that triggers the disassembly of nanoparticles [157,161,162]. This selectivity

prevents the premature drug release in blood circulation, minimizes off-target toxicity and ensures a higher concentration of the drug at the target site. Redox-responsive nanoparticles can also address multidrug resistance by facilitating intracellular accumulation of the drug payload thereby enhancing the efficacy of cancer treatments.

Natural polysaccharides as biomaterial has shown immense potential in the development of nanosized drug delivery platforms [163] owing to their biocompatibility, biodegradability, and non-toxicity [94,95]. Polysaccharide such as chitosan and their derivatives have been extensively explored for the development of nanomedicine responsive to tumor microenvironments [164–166]. Chitosan, a cationic biopolymer derived from chitin when used in the fabrication of nanoparticles, interacts with negatively charged cell membranes and enhances their cellular internalization [125,167]. Chitosan can also be modified to achieve specific properties for drug delivery applications [158,168]. Conjugating a hydrophobic moiety like D-alpha-tocopherol (Vitamin E), on the hydrophilic chitosan backbone may render the conjugate amphiphilic for improving the loading of poorly aqueous soluble drugs [126,132,169]. Vitamin E also modulates signaling pathways such as the PI3K/AKT/mTOR pathway involved in cancer progression and drug resistance [170]. Besides, the ability of Vitamin E to neutralize reactive oxygen species (ROS) that promotes drug resistance in cancer cells, also contributes in overcoming drug resistance by modulating the tumor microenvironment [171–174]. Another amphiphilic derivative of Vitamin E is D-alpha-tocopheryl polyethylene glycol 1000 succinate (TPGS) that provides steric stabilization to nanoparticles, prevents aggregation, and enhances cellular uptake [175,176]. It forms a hydration layer around the nanoparticles, reducing particle-particle interactions and provides stealth against immune recognition, thereby prolonging their circulation in bloodstream [177]. TPGS also provides a reactive terminal functional group for ligand conjugation on the surface of

nanomedicine [176]. Moreover, CSVE and TPGS together can form a mixed micellar structure due to a common hydrophobic core (Vitamin E) that provides better hydrophobic microenvironment for encapsulation and stabilization of hydrophobic drugs in their core [169,175]. CSVE/TPGS-based mixed micelles can also be combined with other polysaccharides like Hyaluronic acid to create hybrid nanostructure with improved performance [178]. Hyaluronic acid (HA), an anionic polysaccharide can enhance the stability of CSVE/TPGS- based micelles as carrier [179,180]. The positive and negative charges of chitosan and hyaluronic acid interact to form a complex that strengthens to self-assemble into nanoparticles through ionic gelation [181]. Hyaluronic acid (HA) also has the ability to interact with CD44 receptors, which are overexpressed on cancer cell surfaces [159,179,180]. Thus, incorporation of HA into nanocarriers can provide targeted drug delivery to the tumor [159,182]. HA also enhances the penetration of nanoparticles into tumor tissue, ensuring better distribution of therapeutic payload in the complex tumor microenvironment. Furthermore, crosslinking of these hybrid structures can be achieved using a crosslinker like 3,3'-Dithiodipropionic acid (DTPA, a redox-responsive linker) [183,184], that utilizes free amine group of CSVE structure to form a stable and compact nanostructure with redox-responsive characteristics.

In present study, Cabazitaxel, an FDA-approved antineoplastic agent, was used as model hydrophobic drug [185]. It disrupts microtubule dynamics in cancer cells, inhibiting mitosis and causing apoptosis [186]. Currently approved for metastatic castration-resistant prostate cancer, it is used in patients who have previously received docetaxel-based chemotherapy [187,188]. However, studies are ongoing to explore its use in other cancer types and its potential in combination with other therapeutic agents [189]. Also, cabazitaxel belonging to BCS Class IV drug exhibit limited aqueous solubility and poor permeability [111]. In addition, associated toxicity to major organs due to non-selective

distribution other than tumor site is another major challenge. Thus, strategies to improve the properties of cabazitaxel for smoothening the delivery is required that can be attained by formulating their nanoparticles. Nanoparticles may address the above issues and ensure higher therapeutic response by minimizing off target distribution, prolonging systemic circulation, controlling drug release and facilitating accumulation to tumor site [111,190]. The nanoparticles can be modified with stimuli responsive and targeting moiety to further specify their delivery to tumor microenvironment and cancer cells, thereby reducing off target distribution and drug-associated adverse effects [191–193]. Current study involves synthesis of Vitamin-E conjugated Chitosan (CSVE). Synthesized CSVE and HA were used for development of TPGS-COOOH stabilized sub -200 nm sized self-assembled hybrid nanoparticle. The prepared particle was further crosslinked with DTPA to endow redox-responsive characteristics. The particles were subsequently functionalized by conjugating Cetuximab on the surface to further improve the selectivity of the nanoparticles toward cancer cell (Schematic illustration of synthesis of CSVE conjugate and TPGS-COOH, and preparation redox responsive nanoparticles; **Figure 5.1**).

5.2 Materials and Methods

5.2.1 Materials

D-alpha-Tocopheryl polyethylene glycol 1000 succinate (TPGS) was obtained as a gift sample from Antares Health Products, St. Charles, USA. Cabazitaxel was a gift sample from Hetero Labs, India. Sodium Hyaluronate (HA), average molecular weight ~9.4 kDa was provided as a gift sample by Shandong Topscience Biotech Co. Ltd., Shandong, PRC. All the other chemicals and solvents used in the experiments were of high purity grade.

The MDA-MB-231, T47D, and HCT116 cell lines were procured from NCCS Pune, India. DMEM (Dulbecco's Modified Eagle Medium), 12-well and 6-well cell culture plate were procured by Genetix (Genetics Biotech Asia Pvt. Ltd). 96 well plates and T-25 flasks

were obtained from Eppendorf. Penicillin-streptomycin, Trypsin-EDTA and FBS (Fetal Bovine Serum) were purchased from Gibco.

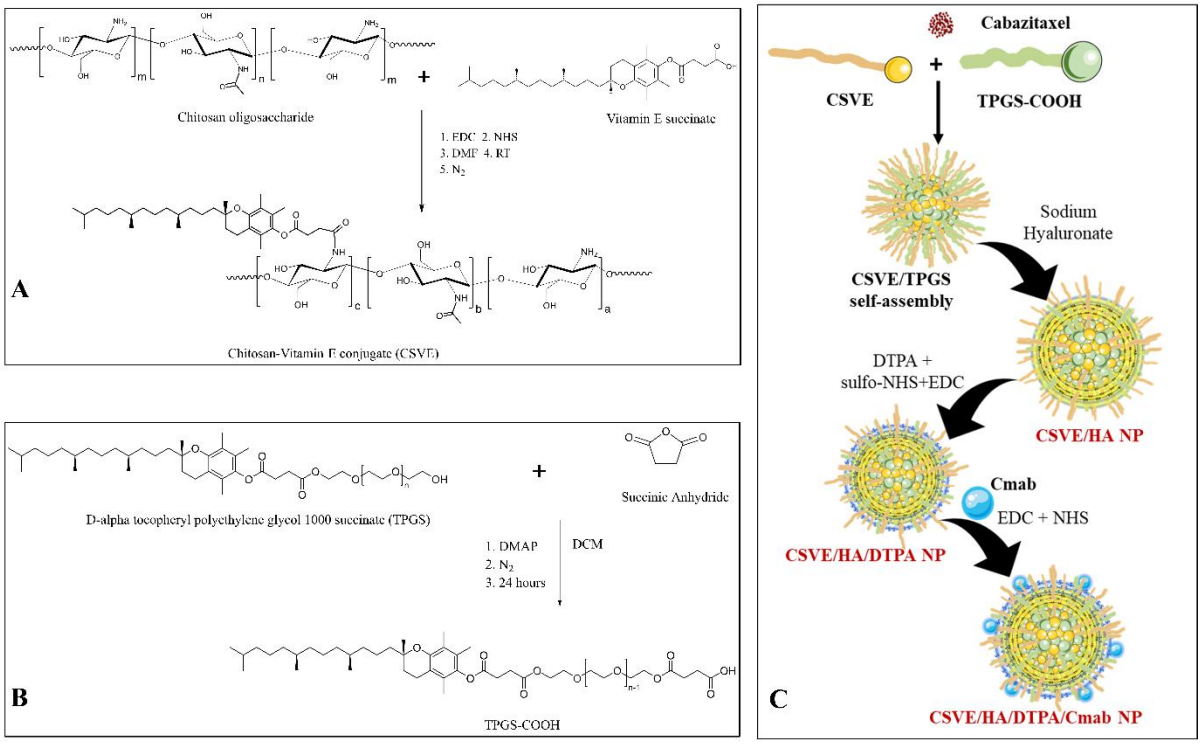

Figure 5.1 Schematic representation of Synthesis of CSVE **(A)** and TPGS-COOH **(B)**; Preparation of CSVE/HA-based redox responsive nanoparticles **(C)**.

5.2.2 Synthesis and Characterization of TPGS-COOH and CSVE

To synthesize succinylated TPGS, 201 mg of SA and 123 mg of DMAP were dissolved in anhydrous DCM. Subsequently, 3 g of TPGS (2 mmol) was dissolved in 30 mL of anhydrous DCM and added to the above reaction mixture. The reaction mixture was purged with Nitrogen gas and maintained under a Nitrogen environment with constant stirring for the complete reaction time of 24 h at 25 °C. Then, the reaction mixture was precipitated in cold diethyl ether, and dialyzed with distilled water for 48 h using Spectra/Por® 7 dialysis membrane (MWCO; 1kDa). The purified solution was lyophilized to yield succinylated TPGS (TPGS-COOH) [114].

For synthesis of CSVE, 106 mg of VES (0.2 mmol), 383 mg of EDAC (2 mmol), and 230 mg of NHS were added in 10 mL of anhydrous DMF under constant stirring. The reaction mixture was purged with Nitrogen gas and maintained under a Nitrogen environment. Then, 168 mg of Chitosan (equivalent to 1 mmol of glucosamine unit) dissolved in 10 mL of anhydrous DMF was added to the reaction mixture under constant stirring in the dark. The reaction continued for 24 h at 25 °C under an inert nitrogen environment. After 24 h, the reaction mixture was concentrated in a vacuum and precipitated in cold diethyl ether. The precipitation was allowed to complete overnight at -80 °C. The precipitated product was washed with ethanol three times. The washed product was consecutively dialyzed using Spectra/Por® 7 dialysis membrane (MWCO; 1kDa) against a water-ethanol mixture (1:1 v/v ratio) and distilled water for 24 h each. The dialyzed solution was then lyophilized after freezing it overnight at -80 °C to yield D-alpha-Tocopherol succinate conjugated chitosan (CSVE) [126,132].

Characterization of TPGS-COOH and CSVE was done using Fourier transform infrared (FTIR) and nuclear magnetic resonance (NMR) spectroscopy to validate the succinylation of TPGS and conjugation between VES and chitosan. FTIR spectrum of TPGS, TPGS-COOH, CSO, and CS-VE was recorded on Nicolet iS5 (Thermo Electron Scientific Instruments LLC) while their ^{1}H and ^{13}C NMR spectrum were acquired using a Bruker 500 MHz NMR Spectrometer (AVH D 500 AVANCE III HD; BRUKER BioSpin International AG). TPGS and TPGS-COOH were analysed as detailed in **section 4.3.1**. To analyze CSO and CS-VE were dissolved in deuterated DMSO (d-6 DMSO).

5.2.3 Formulation of CSVE-based nanoparticles

The hybrid CSVE/HA nanoparticles (CSVE/HA-NP) were prepared using the solvent emulsification-evaporation method. Briefly, the CSVE conjugate (detailed in supplementary) and TPGS was dissolved in 10 ml of distilled water and kept on stirring.

CBT (5mg ml^{-1}) in chloroform was added to the CSVE/TPGS solution and probe sonicated using 6 mm probe at 70% amplitude for 7 minutes on ice-bath [126]. The solution was kept on stirring at 200 rpm for 3 h for the organic solvent to evaporate. The anionic TPGS and cationic CSVE forms stable micellar assembly due to their amphiphilic nature and common hydrophobic group. Subsequently, 5 ml of HA solution in distilled water (2 mg ml^{-1}) was added dropwise and stirred for 2 h [194].

To prepare redox-responsive nanoparticles (CSVE/HA/DTPA NP), only 2.5 ml of HA (2mg ml^{-1}) was used, while DTPA was used as crosslinker according to previously reported method with minor modification [160,195]. For this, 72 mg of sulfo-NHS and 64 mg of EDC was dissolved in 2.5 ml of water and 12 mg of DTPA was added, stirred for 30 min. This solution was added dropwise into the CSVE/HA nanoparticles suspension and stirred for 3 h. For the preparation of targeted nanoparticles (CSVE/HA/DTPA/Cmab), CSVE/HA/DTPA was incubated with NHS and EDC for 30 minutes followed by the addition of Cetuximab (2.5 mg) and stirred for 3 h [120]. The nanoparticles were washed thrice with distilled water using Amicon® ultra centrifugal filters (MWCO 30 kDa). The washed nanoparticles were then subjected to lyophilization and stored at 4-8 °C until further use. In preparing coumarin-6 (CM6) loaded nanoparticles 0.3 mg of CM6 was added instead of cabazitaxel to the 1 ml of chloroform mentioned above. Also, for preparing chitosan -based hybrid nanoparticles, CSVE was replaced with water soluble CSO.

5.2.4 Characterization of CSVE-based nanoparticles

5.2.4.1 Assessment Hydrodynamic particle size, zeta-potential, and particle morphology

The size and zeta potential (ζ) were determined using Malvern Zetasizer (Nano ZS90, Malvern Instruments). The morphology of the nanoparticles was evaluated by

Transmission Electron microscope (TEM) Tecnai G2 20 TWIN (FEI, USA), Scanning Electron Microscope (SEM) Nova Nano SEM 450 (FEI, USA), and Scanning Probe Microscope (SPM/AFM) NTEGRA Prima (NT-MDT Service & Logistics Ltd.).

5.2.4.2 Analytical Method Development of Cabazitaxel

The analytical method of cabazitaxel was developed on a High-Performance Liquid Chromatography (HPLC) instrument (Shimadzu, Japan). The C18 column (150 mm length, 4.6 mm diameter, and 5 µm particle size) was used to develop the analytical method of cabazitaxel. The instrument was attached to a DAD detector and 229 nm was the wavelength used to estimate cabazitaxel concentration. The mobile phase of Acetonitrile (ACN) and 0.3 % acetic acid in water (W0.3aa) at 0.76 and 0.24 volume fractions respectively. The flow rate was maintained at 1 ml min-1. The HPLC chromatogram of Cabazitaxel is provided previously in **Figure 4.2** of Objective 1.

5.2.4.3 Estimation of Encapsulation Efficiency

The encapsulation efficiency of the nanoparticles was calculated using the analytical method. Briefly, the 10 mg of nanoparticle was added in 2 ml of ACN and bath sonicated for 30 minutes. The solution was then filtered using a 0.1 µm pore-size syringe filter. The filtered solution was then analyzed using HPLC to estimate the amount of encapsulated drug. The percentage of drug loading was also calculated using the data from the calculation of the amount of encapsulated drug.

5.2.4.4 Bradford assay to determine degree of cetuximab conjugation.

Bradford assay was used to estimate the cetuximab concentration in the purified nanoparticle [139]. A UV-Spectrophotometer-based analytical method was developed to estimate proteins using bovine serum albumin (BSA) as standard. Briefly, various dilutions of BSA were mixed with Bradford's reagent and allowed to rest for 5 minutes. The absorbance was noted at 595 nm wavelength using a UV-Spectrophotometer. The

concentration-absorbance curve obtained from the experiment was used to estimate cetuximab conjugated on the surface of the prepared nanoparticles.

5.2.4.5 Solid-state characterization (XRD, FTIR, DSC, and XPS)

Fourier-transform infrared (FT-IR) spectra of pure drug (CBT), CSVE, HA, TPGS (TPGS-COOH) and all the formulations were acquired using a JASCO FT/IR-4200 type A (JASCO Co., Tokyo, Japan) using KBr method. All spectra were scanned in the range 600–4000 cm−1. Differential scanning calorimetry (DSC) was performed using DSC-60 Plus (Shimadzu, Asia Pacific). 5mg of lyophilized sample was filled in the sealed aluminum pans and analyzed under nitrogen atmosphere at 10 °C/min from 0 to 250 °C. X-ray diffraction (XRD) analysis of lyophilized samples was done using the Rigaku Miniflex 600 Desktop X-Ray Diffraction System (RIGAKU Corporation). Monochromatic CuKα-radiation (λ = 1.5406 Å) was used at 40 mA and at 40 kV over a range of 2θ angles from 0° to 50° with an angular increment of 0.02°/s and scan speed of 1°/min. X-ray photoelectron spectroscopy (XPS) was used to assess the surface chemistry of the formulations. The pellets of lyophilized formulation were used to obtain the spectra on K-Alpha (Thermo Fisher Scientific) with Mg Kα radiation (hν = 1253.6 eV) in the range of 100-700 eV binding energy.

5.2.5 Drug release Study

Drug release studies were performed using the dialysis method [196]. Herein, the nanoparticle suspensions equivalent to 5 mg of Cabazitaxel were loaded in a sealed pouch of dialysis membrane (Spectra/Por® 7 1000 Da MWCO) and immersed in 50 ml of media. 1 ml of media was collected at predetermined time intervals. The samples were then filtered with 0.1 µm pore size membrane filters and analyzed using the HPLC-based analytical method. The drug release was investigated in phosphate buffer saline (pH 7.4), Acetate Buffer (pH 5.5), and Acetate buffer (pH 5.5)/GSH (10mM).

5.2.5.1 Ellman's assay for in-solution quantification of sulfhydryl groups

Ellman's reagent is 5,5'-dithio-bis-(2-nitrobenzoic acid), also known as DTNB, a compound used for quantitating free sulfhydryl groups in solution. DTNB produces a yellow-colored product on reacting with sulfhydryl groups, that can be quantified by measuring absorbance at 412 nm using a spectrophotometer.

Ellman's Reagent was used to determine the redox responsive behavior of CSVE/HA/DTPA NP. Firstly, Ellmans reagent (80µg/ml) in buffer solutions (0.1 M sodium phosphate, pH 8.0, containing 1 mM EDTA) was prepared. Then, 300mg of CSVE/HA/DTPA NP weigh was incubated in 20 ml of acetate buffer (pH 5.5) with GSH (150 mg; ~0.5 millimole). 250µl of aliquots were collected at 5, 15, 30, 45, 60, 90, and 120min and samples were incubated with 2.5ml of Ellman's Reagent Solution for 15 min. 200 µl incubated solution was transferred in 96 well plate and absorbance were measured at 412nm using microplate reader. The absorbance vs time graph was plotted.

5.2.6 Stability of lyophilized nanoparticles

To assess the stability of the prepared formulations washed and purified CSVE/HA/DTPA NP and CSVE/HA/DTPA/Cmab NP were lyophilized and packed in airtight borosilicate glass vials and kept in refrigerator at 4 °C for predetermined intervals. After day 7, 15, 30, 90, and 180, the lyophilized formulation was resuspended in deionized water and assessed for hydrodynamic particle size, zeta potential, PDI, and entrapment efficiency.

5.2.7 In vitro cell line studies

5.2.7.1 Cell line maintenance

The MDA-MB-231, T47D, and HCT116 were incubated in a humidified CO_2 incubator at 37 °C while being cultured in DMEM with FBS (Fetal Bovine Serum) and penicillin-streptomycin solution.

5.2.7.2 Cytotoxicity assay

The cytotoxicity of the prepared formulations were examined by MTT (3-(4, 5-dimethylthiazolyl-2)-2, 5-diphenyltetrazolium bromide) assay [197]. The cytotoxicity of the prepared formulations were examined MDA-MB-231, T47D, and HCT-116 cells [197]. The cells were grown in an incubator at 37 °C under 5% CO_2 condition with their respective media. After the cells were harvested, they were counted and seeded at 1 × 10^5 cells per well in a 96-well plate overnight. The following day, cells were exposed to various concentrations of Blank Formulation, Standard (Cabazitaxel), cabazitaxel loaded hybrid CSO-HA nanoparticle (CSO/HA NP), cabazitaxel loaded hybrid CSVE-HA nanoparticle (CSVE/HA NP), cabazitaxel loaded redox responsive hybrid CSVE-HA nanoparticle (CSVE/HA/DTPA NP) and Cetuximab conjugated cabazitaxel loaded redox responsive hybrid CSVE-HA nanoparticle (CSVE/HA/DTPA/Cmab). Then, the treated cells were incubated for 24 h. Following incubation, 100 µL of (5 mg/mL) MTT reagent dissolved in media was added to each well and then cells were incubated for another two hours. Subsequently, the solution was removed and 100 µL of dimethyl sulfoxide (DMSO) was added to the wells. Afterward, the plate was read at 570 nm using a microplate reader. The following formula was used to determine the percentage of viable cells:

$$\text{Percentage of viability (\%)} = \frac{(\text{Absorbance of sample at 570 nm})}{(\text{Absorbance of control at 570 nm})} \times 100$$

5.2.7.3 Cellular uptake

Cellular uptake studies used Coumarin-6 (CM6)-loaded formulations and free coumarin6 (CM6). 5× 10^4 MDA-MB- 231 cells were seeded in 12 well culture plates and incubated to adhere for 24 h. The cells were treated with CM6-loaded formulations equivalent to 2 µg ml^{-1} of CM6 and free CM6 dissolved in complete DMEM for six hours and incubated at

37 ºC. To assess the role of EGFR in endocytosis of nanoparticles, one of the wells received cetuximab pretreatment (30 mins before the formulation treatment). Cells were washed with PBS and stained with Hoechst33342 (10 µg ml^{-1}) to incubate for 20 minutes for nuclear staining. Subsequently, stained cells were washed with PBS, and images were captured in green and blue channels EVOS FL Cell Imaging System. Further, a quantitative assessment of cellular uptake was performed using flow cytometry. Similar steps were performed up to the treatment stage. After the treatment with formulations, the cells were harvested in 1 mM EDTA and rinsed twice with PBS. The fluorescence intensity of the CM6 was measured based on cell distribution using Cell Quest Calibur Flow Cytometer (Becton Dickinson, USA) [198]. The experiment was performed in triplicate.

5.2.7.4 Mitochondrial membrane potential and distribution pattern

Briefly, 5×10^4 viable MDA-MB-231 cells were seeded in 6-well cell culture plate and incubated for 24 hrs. Thereafter, the cells were treated with IC_{50} concentrations of formulations and incubated for 24 h. Further, cells were stained with JC-1 dye at 1 µM concentration in PBS and incubated for 30 minutes at 37 ºC. Finally, the images were taken by fluorescence microscope. The changes in mitochondrial membrane potential were validated quantitatively through flow cytometry. For quantitative detection, a similar experimental procedure was followed. The cells were harvested in 1 mM EDTA solution in PBS, stained with JC- 1 dye, and analyzed using flow cytometer [199].

To evaluate the mitochondrial distribution pattern, similar protocol was followed up to the treatment stage. Following treatment, the cells were stained with MitoTracker™ Red at 1 µM concentration and counterstained nucleus using Hoechst33342 at 10µg ml^{-1} concentration for 30 minutes. After staining the cells were again washed with PBS and the

images were taken by fluorescence microscope in phase contrast, blue and red channels [200].

5.2.7.5 Apoptosis Analysis using Hoeschst33342/PI

Qualitative assessment of apoptosis was done using Hoechst33342 and PI double staining. The MDA-MB-231 cells were plated on 12-well cell culture plate for about 24h. Thereafter, the cells were treated with IC_{50} concentrations of the formulations and incubated for 24h. Further, PI (5µl) and Hoechst33342 (10µg ml^{-1}) were then added to the wells of plate and then kept in dark for about 30 minutes at 37°C. The wells were washed with PBS and observed by a fluorescence microscope [201].

For quantitative assessment of apoptosis, Alexa Fluor 488 Annexin V/PI double stained MDA-MB-231 cells were subjected to a flow cytometry after being exposed to IC_{50} concentrations of the formulations. For this, 2×10^5 cells were seeded in 6-well cell culture plates and incubated for 24 hrs. Thereafter, the cells were treated with IC_{50} concentrations of the formulations. After 24 h, cells were harvested in 1 mM EDTA in PBS (pH 7.4). Further, treated and control cells were processed according to the manufacturer protocol for Alexa Fluor 488 Annexin V/PI staining (Thermo Fisher Scientific, Invitrogen Bioservices India Pvt. Ltd.). After staining, the samples were analyzed by flow cytometry to evaluate apoptosis [202].

5.2.8 In vivo Studies

All *in vivo* experiments were carried out in accordance with the guidelines of CPCSEA (a Committee for the Purpose of Control and Supervision of Experiments on Animals, Regd. No. 2123/GO/Re/S/21/CPCSEA). The protocols for *in vivo* studies were approved by Institutional Animal Ethics Committee (IAEC) (Approval number: IIT(BHU)/IAEC/2022/011) prior to conduction of experiments. The animals were

procured from animal facility, Institute of Medical Sciences (BHU), Varanasi-221005 (542/GO/ReBi/S/02/CPCSEA).

5.2.8.1 Tumor Induction in Female SD Rats

Female Sprague-Dawley rat pubs of 5 weeks age (weight 50–60 g) were used to develop a DMBA-induced mammary tumor model. After 1 week of conditioning under light and dark conditions for 12 h (age 6 weeks), all the rats received 7,12-Dimethylbenz(a)anthracene dissolved in corn oil (dose 80 mg kg^{-1}) by subcutaneous injection into the mammary fat pad [203,204]. After 60 days, the tumors started to appear. The tumor volume was measured regularly. After 90-100 days of the treatment with DMBA, the tumors exceeded volume of 500 mm^3 and they are divided into various groups for studies mentioned below. The tumor volume was estimated using the formula;

$$V = \frac{4}{3}\pi(r^3)$$

where r indicates the average radius of the tumor tissue

5.2.8.2 Pharmacokinetic studies

A pharmacokinetic study was performed on healthy female SD rats. The tumor-bearing rats were randomly distributed in 3 groups (n = 12). Group 1 to 3 received micellar Cabazitaxel (CBT), CSVE/HA/DTPA, and CSVE/HA/DTPA/Cmab, respectively via intravenous injection into tail vein at a dose equivalent to 10 mg kg^{-1} of Cabazitaxel. The blood samples (200 µL) were collected under the mild anesthetic condition through *oculi choroideae* and centrifuged at 8000g for 5 min at -4 °C to separate the plasma. The liquid-liquid extraction method was used for plasma sample processing and analyzed by the developed HPLC method (**details in 4.2.9.1**). The plasma concentration-time profile was evaluated using the PK Solver add-in program to determine the pharmacokinetic parameters.

5.2.8.3 Biodistribution studies in tumor-bearing rats

To assess the drug distribution to majorly perfused organs, a biodistribution study was performed in tumor-bearing rats. The animals were divided into 3 groups (n=12). Group 1 received cabazitaxel, group 2 received CSVE/HA/DTPA NP, and group 3 received CSVE/HA/DTPA/Cmab NP at a dose equivalent to 10 mg kg^{-1} of Cabazitaxel via. intravenous route. After administration of the dose, animals were euthanized at predetermined time intervals. Liver, lung, kidney, spleen, and tumor tissues were collected from animals of each group after 2, 10, 24, and 48 hours of drug administration. 200 mg tissue sample was weighed and homogenized at -4°C. The drug content from the homogenate was extracted using solvent extraction. A 1:1 (v/v) mixture of acetonitrile and methanol (200 µl) was added in the homogenate and mixed. The homogenate was separated by centrifugation and the supernatant was analyzed for drug concentration using HPLC method.

5.2.8.4 Tumor Regression Analyses

The animals were divided into four groups (n=5) and CSVE/HA/DTPA NP and CSVE/HA/DTPA/Cmab NP were administered through an intravenous route once every 3^{rd} day for 3 weeks at the dose equivalent to 10 mg kg^{-1} of CBT. The control and standard group were treated with PBS and CBT respectively. The tumor growth was measured every 7 days using Vernier caliper. The animal body weight was also measured throughout the study to check the overall toxicity; one group of healthy rats was used to estimate the weight change in normal rats [205,206]. Finally, the animals were killed after 28 days, and the tumor was collected for histological studies.

5.2.8.5 Survival Analysis

For survival analysis, the tumor-bearing female SD rats were divided into four groups (n=5) and healthy female SD rats in one group. The animals were treated with the same

regimen mentioned in the tumor regression study. The survival study was carried out for up to 120 days. Finally, the dignified survival rate was evaluated with the use of the Kaplan-Meier analysis [207].

5.2.8.6 Assessment of acute toxicity by histological examination organs and tumor

After the tumor regression study, the rats were sacrificed. Major organs and tumors were collected. The collected samples were separately fixed in 10% paraformaldehyde (PBS buffer) for 12 h. The tissues were dehydrated, treated with xylene and embedded in paraffin blocks. The wax blocks were sectioned using a microtome (Leica) to obtain 5 μm thick sections. These sections were deparaffinized and then subsequently exposed to hematoxylin and eosin staining protocol. The stained section was then dehydrated again and cleared with xylene, and mounted under a coverslip to visualized under a light microscope for histological changes [143,146,208].

5.2.9 Statistical Analysis

The results were reported as Mean ± standard deviation (SD). The statistical significance of data was determined using t test (non-parametric), one-way ANOVA and two-way ANOVA at p values of *p<0.05, **p<0.01, ***p<0.001, and ****p<0.0001. all statistical analysis were performed using GraphPad Prism 9.0.0 for windows (GraphPad Software, San Diego, CA, USA).

5.3 Results and Discussion

5.3.1 Synthesis of TPGS-COOH and CS-VE

The synthesis was confirmed by FTIR (**Figure 5.2**) and NMR spectra (**Figure 5.3 & Figure 5.4**). In FTIR spectrum, characteristic peaks for TPGS were observed at 3500 cm^{-1} for terminal -OH group, 2917 cm^{-1} for alkyl -CH stretching bond of aliphatic parts of the molecule, 1742 cm^{-1} and 1646 cm^{-1} for -C=O stretching vibration, 1464 cm^{-1} for –C=C– peak of aromatic ring, 1351 cm^{-1} for peculiar peak of $–CH_2$ group of PEG chain, 1280 and

1115 cm^{-1} for -C-O- stretching peaks. For TPGS-COOH, peaks were observed for terminal hydroxyl functional band at 3485 cm^{-1}, –CH stretching vibration of the methyl group at 2909 cm^{-1}, strong –C=O stretching vibration at 1734 with increased transmittance and peak at 1645 cm^{-1} confirmed successful synthesis of TPGS-COOH, –C=C– peak of aromatic ring at 1465, $–CH_2$ peak of PEG chain at 1353, -C-O- stretching at 1106.

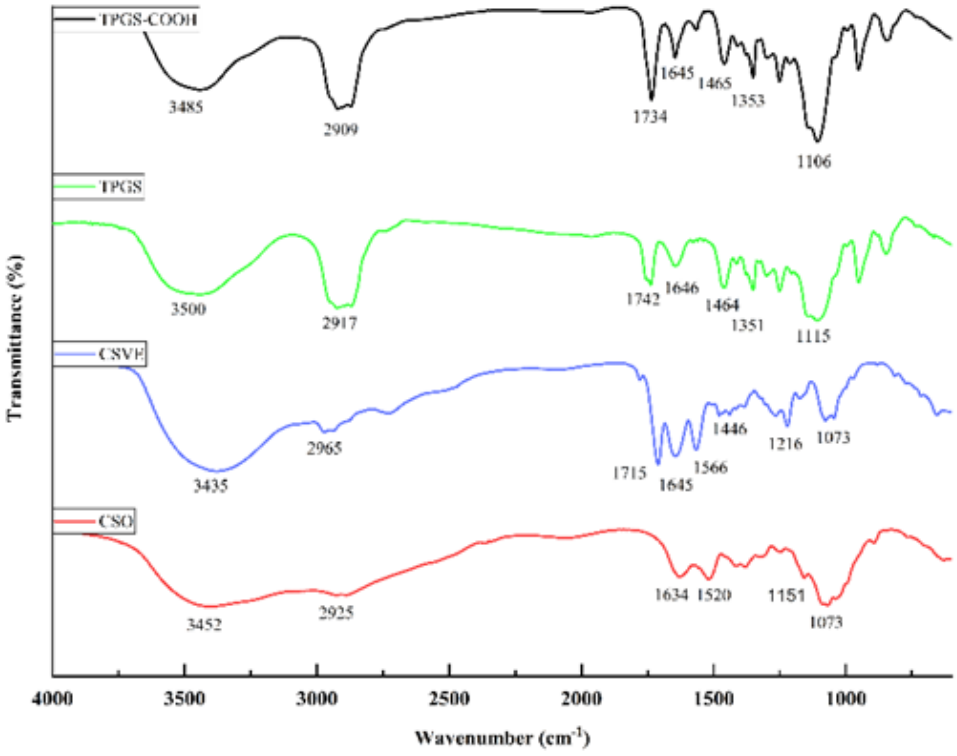

Figure 5.2 FTIR spectra of TPGS, TPGS-COOH, CSO, and CSVE.

Chitosan exhibited characteristic peak at 3452 cm^{-1} as broad peak for hydroxyl (-OH) stretching and NH_2 group, 2925 cm^{-1} for C-H stretching, 1634 cm^{-1} for C=O stretching vibrations of N-acetylated unit of chitosan, 1520 for -NH bending, 1151 and 1073 cm^{-1} for C-O-C stretching vibrations. CSVE showed characteristic carbonyl peaks at (-C=O) at 1715 cm^{-1} and 1645 cm^{-1} (increased intensity), indicating the conjugation of acid terminal of VES to amine terminal of chitosan [132]. CSVE also showed a characteristic peak at 1566 cm^{-1} corresponding to C=O stretching vibrations of ester group of VES

[138]. Reduction in free amine groups due to successful conjugation of VES and CS resulted in shielding of peak around 1520 cm^{-1} observed with CSO for NH bending. The obtained peaks indicated the successful linkage between VES and chitosan via amide bond formation.

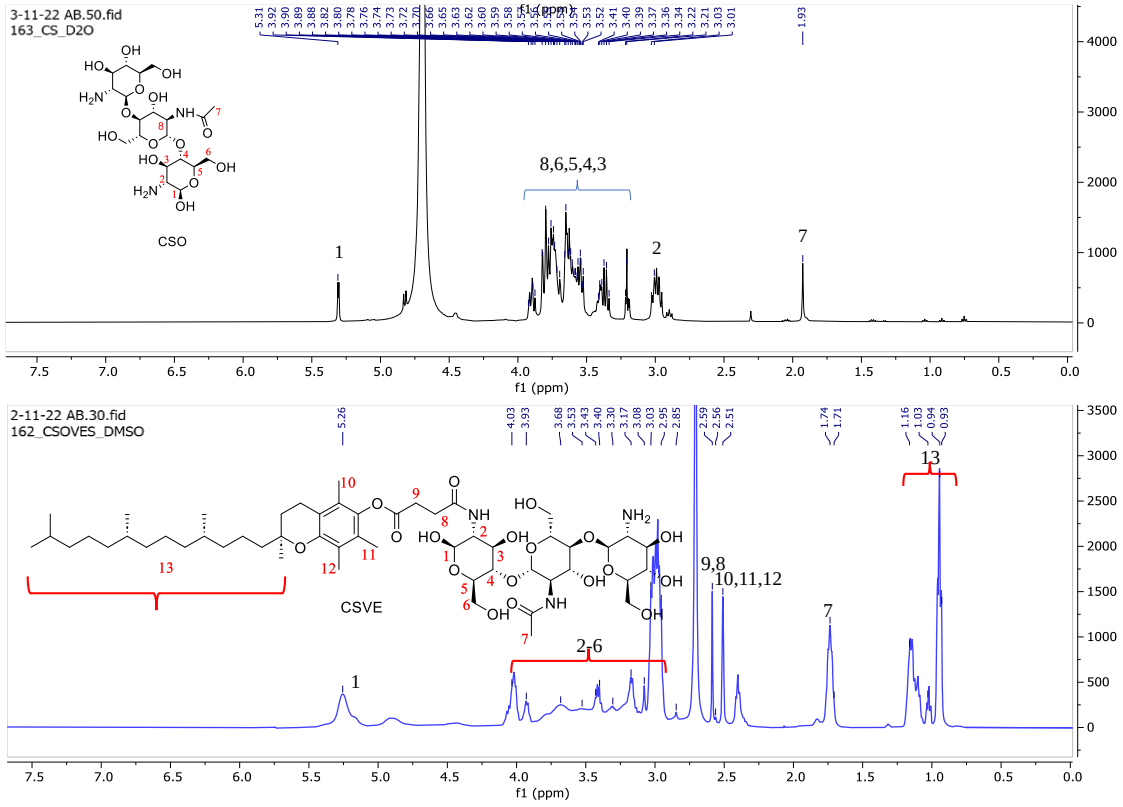

Figure 5.3 The ^{1}H NMR spectra of CSO (black) and CSVE (blue).

The ^{1}H NMR spectra confirmed the successful synthesis of CSVE, as shown in **Figure 5.3**. Chitosan showed characteristic anomeric proton peak at 5.31 ppm (1). The peak at 3.0 ppm was of -C2 of glucosamine (2), while protons of C3-6 is observed in the range of 3.2-3.9 ppm. The proton of C8 i.e., C2 of acetylated glucosamine unit was also observed in the same range. The 1.93 ppm peak was of the terminal methyl group (C7) of acetylated glucosamine unit.

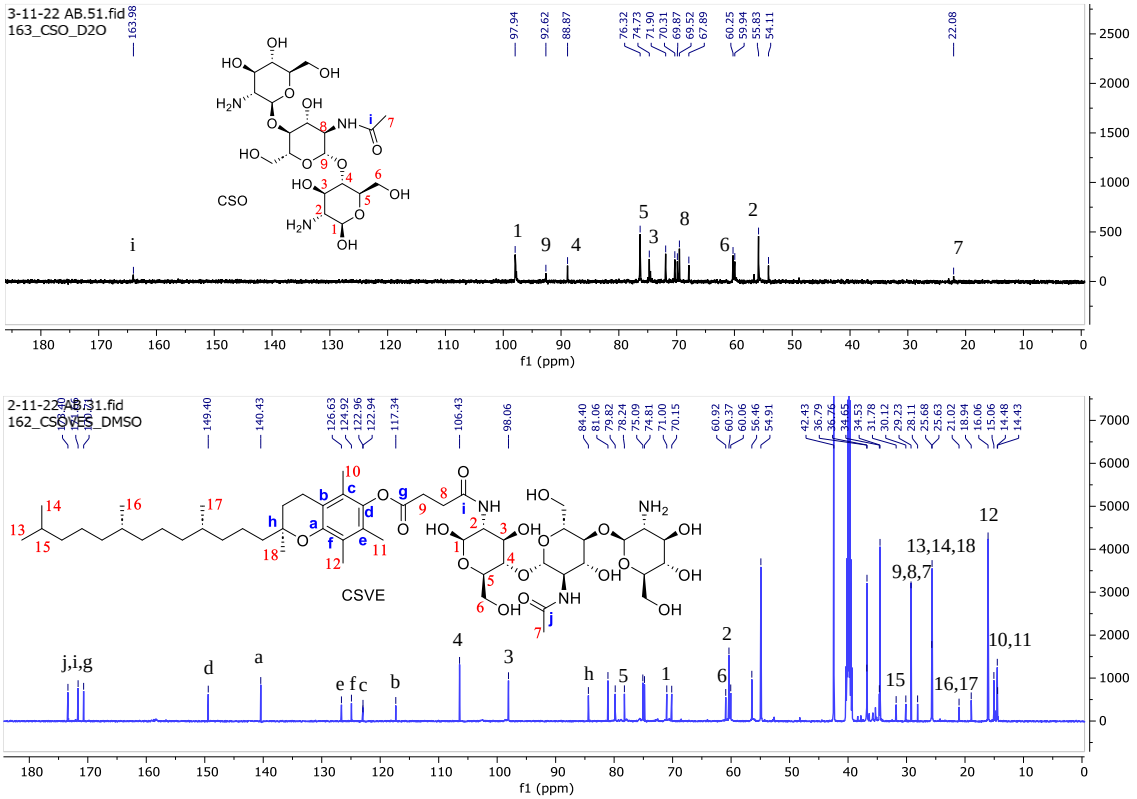

Figure 5.4 The ^{13}C NMR spectra of CSO (black) and CSVE (blue).

For CS-VE, the methylene proton (8,9) of succinyl group of VES and protons of -CH3 attached to the aromatic ring (10-12) was observed at 2.59 ppm and 2.51 ppm respectively. The peak in range of 0.9-1.3 ppm was for methyl proton of long aliphatic chain of VES (13) while peak at 2.85-4.03 ppm was for anomeric carbon protons of C3-6 (2-6) of CSO. The proton (7) of acetyl group attached to amine group was also observed in CSVE at 1.7 ppm. The results confirmed the successful synthesis of CSVE and were in accordance to previous reports [114].

Figure 5.4 shows ^{13}C NMR spectra of CSO and CSVE. The spectrum of CSO showed characteristic peaks of glucosamine unit in the aliphatic region (1-6, 8, 9). Also, the carbonyl carbon (i) and methyl group of acetylated glucosamine was observed at 164 ppm and 22 ppm respectively. The spectrum of CSVE showed three carbonyl peaks (j, i, and g) in the range of 170-175 ppm, along with all the characteristic peaks of CSO and

succinylated tocopherol, suggesting the successful conjugation of CSO and VES.

5.3.2 Formulation and characterization of CSVE-based nanoparticles

5.3.2.1 Morphological assessment of the prepared nanoparticles

The prepared conjugate of CSO and CSVE was used to prepare CSVE based nanoparticles. The presence of same hydrophobic group (VES) and the net cationic and anionic charge of CSVE and TPGS-COOH respectively allows the formation of a stable micellar structure in aqueous conditions. The drug (CBT) was loaded in the stable hydrophobic core of the micellar structure which was further stabilized by ionic gelation through the addition of anionic hyaluronic acid. The stable hybrid nanoparticle formed was then crosslinked using the DTPA to endow redox-responsive release behavior via. carbodiimide chemistry. To impart cancer selective characteristics, the particle was surface functionalized by conjugating Cmab to the carboxyl group of TPGS-COOH present on the surface of nanoparticle.

The formulation composition and characterized parameters are as in **Table 5.1** Composition, particle size, polydispersity index (PDI), zeta potential, and entrapment efficiency of various formulations.. The hydrodynamic size determined by DLS of CSO/HA NP, CSVE/HA NP, CSVE/HA/DTPA NP, and CSVE/HA/DTPA/Cmab NP were 190±23 nm, 179±32 nm, 164±29 nm; and 203±43 nm, respectively. The amphiphilic nature of the CSVE conjugate combined with identical hydrophobic segment (VES) of TPGS-COOH allows for the formation of a compactly packed micellar structure that leads to lower size of CSVE/HA NP. The size of CSVE/HA/DTPA NP and CSVE/HA NP did not show major difference. However, the size of CSVE/HA/DTPA/Cmab NP exhibited marked increase that may be attributed to the conjugation of Cmab on the surface of nanoparticle.

However, the zeta potential (ζ) showed a different trend, with CSVE/HA/DTPA NP exhibiting highest zeta potential, followed by CSVE/HA/DTPA/Cmab NP, CSO/HA NP, and least in CSVE/HA NP (**Table 5.1**). This observation may be due to the higher amount of HA (an anionic polysaccharide) being used in CS/HA NP and CSVE/HA NP. The lower ζ in CSVE/HA NP than CSO/HA NP may be due to the crosslinking *via.* amide bond formation between of chitosan and VES. Similar results have been previously reported where ζ has exhibited reduction due to the conjugation of moieties with the amine groups of CSO [114,132]. Polydispersity index (PDI) of all formulations was less than 0.3, indicating monodispersed systems. Additionally, TEM, SEM, and AFM images confirmed the formulation of well-structured spherical nanoparticles (**Figure 5.5**). The particle size of CSO/HA NP, CSVE/HA NP, CSVE/HA/DTPA NP, and CSVE/HA/DTPA/Cmab NP, observed by TEM were 170±12 nm, 135±19 nm; 126±14 nm; and 175±9 nm, respectively. The size observed in TEM was smaller than observed in DLS that could be due to difference in measurement conditions, as TEM analysis was done for dried samples while DLS measured the hydrodynamic size of the particles and takes into account the solvated water molecules on the surface [138].

Table 5.1 Composition, particle size, polydispersity index (PDI), zeta potential, and entrapment efficiency of various formulations.

Formulation	Composition (mg)							Particle size (nm)	PDI	(ζ)	EE (%)	DL (%)
	CSO	CSVE	HA	TPGS-COOH	CBT	DTPA	Cmab					
CSO/HA NP	50	--	10	10	5	--	--	190 ± 23	0.265 ± 0.08	19.2 ± 2.35	53.24 ± 3.57	4.71 ± 0.19
CSVE/HA NP	--	50	10	10	5	--	--	179 ± 32	0.238 ± 0.07	16.4 ± 3.72	62.35 ± 2.91	5.06 ± 0.13
CSVE/HA/DTPA NP	--	50	5	10	5	12	--	164 ± 29	0.268 ± 0.05	12.1 ± 2.08	64.49 ± 3.53	4.98 ± 0.07
CSVE/HA/DTPA/Cmab NP	--	50	5	10	5	12	2.5	203 ± 43	0.167 ± 0.06	11.9 ± 2.57	63.77 ± 3.96	4.85 ± 0.14

EE(%) = Entrapment efficiency

DL(%) = Drug Loading

(ζ) = Zeta potential

*Results are shown as Mean ±SD (n=6).

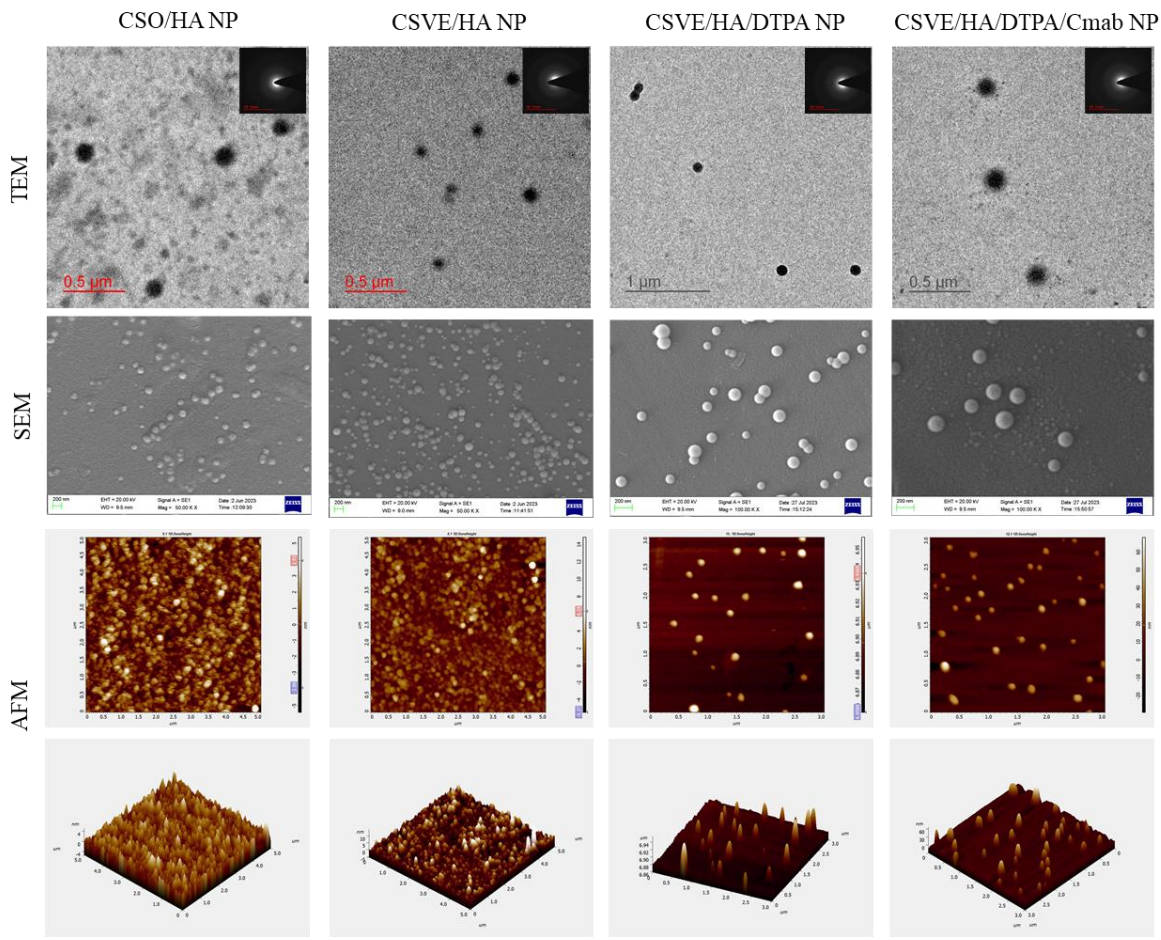

Figure 5.5 Morphological assessment (TEM, SEM, and AFM) of CSO/HA NP, CSVE/HA NP, CSVE/HA/DTPA NP, and CSVE/HA/DTPA/Cmab NP.

The SAED pattern for all nanoparticles exhibited diffused rings, reflecting the amorphous state of nanoparticles. The particles of spherical anisotropy were confirmed by SEM (i.e., CSO/HA NP: 145±24, CSVE/HA NP: 136±22 nm, CSVE/HA/DTPA NP: 117±21 and CSVE/HA/DTPA/Cmab NP: 152±29) and were of size similar to TEM results. TEM and SEM results followed the trend of DLS results, as desired. AFM images further confirmed the smooth surface spherical morphology of formulated nanoparticles. The results of SEM, TEM and AFM were in good correlation. The entrapment efficiency of formulated nanoparticles ranged between 53-65%. The nanoparticles formulated using synthesized CSVE/HA had higher entrapment than CSO/HA nanoparticles. The higher entrapment of

CSVE based formulations than CSO/HA NP may be attributed to the amphiphilic nature of synthesized CSVE that may improve the drug loading capacity for hydrophobic drugs in the core of the micellar structure [114]. The degree of Cmab conjugation to the carboxyl group of TPGS-COOH was confirmed by Bradford assay (detail in supplementary) that showed 71.635±4.23 % of added Cmab was conjugated on surface, indicating efficient surface functionalization.

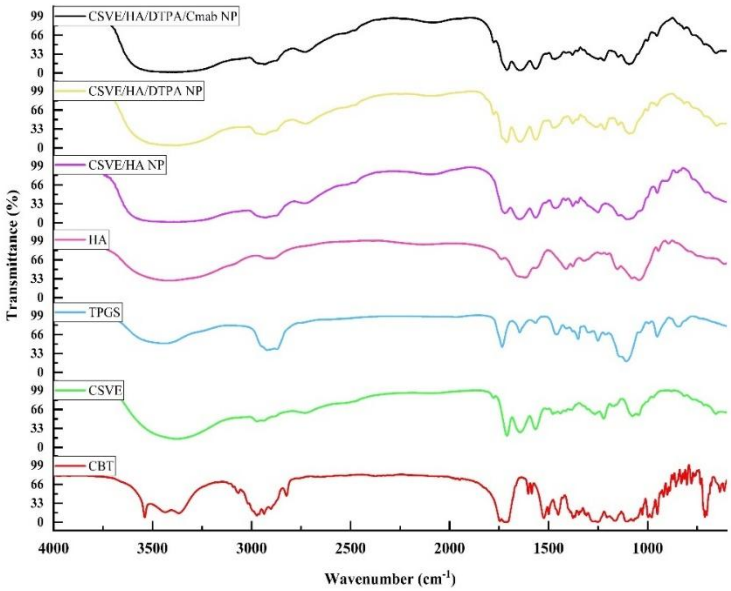

Figure 5.6 The FTIR spectra of CBT, CSVE, TPGS, HA, CSVE/HA NP, CSVE/HA/DTPA NP and CSVE/HA/DTPA/Cmab NP.

5.3.2.2 Solid-state characterization (FTIR/ XRD/DSC/XPS)

The FTIR spectra of CBT, CSVE, TPGS, HA, CSVE/HA NP, CSVE/HA/DTPA NP and CSVE/HA/DTPA/Cmab NP were as shown in **Figure 5.6.** The FTIR spectra of CBT, CSVE, TPGS, HA, CSVE/HA NP, CSVE/HA/DTPA NP and CSVE/HA/DTPA/Cmab NP were as shown in Fig. 2A. The characteristic peaks of CBT were observed at 3539 cm−1, 3441 cm−1, 3368 cm−1, 3070 cm−1, 2974 cm−1 (a strong peak for N-H stretching of 2˚ amine), 2821 cm−, 2746 cm−1, 1748 cm−1, 1713 cm−1, 1525 cm−1 (C=C Stretching),

1499 cm−1, 1452 cm−1 (-CH3 bending), 1379 cm−1 (-C-N Stretching), 1280 cm−1, 1159 cm−1, 1103 cm−1, 977 cm−1, 949 cm−1, and 714 cm−1 (C-H stretching of benzene).

The peaks were similar to previous reports for CBT [105,209,210]. FTIR spectra of TPGS and CSVE were as discussed above. The FTIR peaks of HA were at 3467 cm−1 corresponding to -OH stretching as broad band, 2927 cm−1 for symmetric methyl -C-H stretch, 1600 cm−1 and 1400 cm−1 were correlated to C-O stretching of COO-, while 1067 cm−1 cm−1 was linked to C-O-C hemiacetalic system of saccharide units [73,74]. The FTIR spectrum of CSVE/HA nanoparticles exhibited merged peaks of CSVE and HA and similar trend was followed by CSVE/HA/DTPA NP and CSVE/HA/DTPA/Cmab NP. The characteristic peaks of crystalline CBT were masked by CSVE and HA, indicating complete encapsulation of drug in prepared nanoparticles.

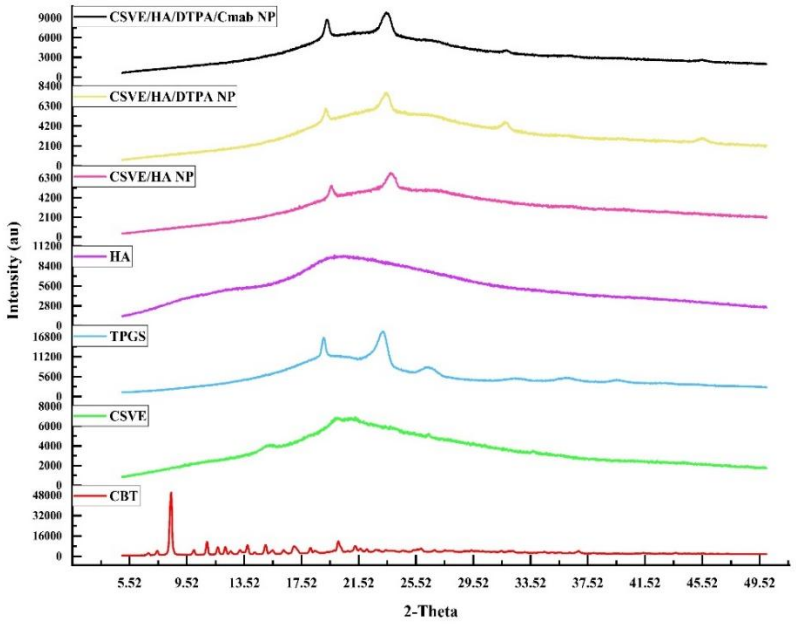

Figure 5.7 The XRD spectra of CBT, CSVE, TPGS, HA, CSVE/HA NP, CSVE/HA/DTPA NP and CSVE/HA/DTPA/Cmab NP.

The characteristic peaks observed for CBT were similar to previous reports for CBT [105,209,210]. The FTIR spectrum of CSVE/HA nanoparticles exhibited merged peaks of

CSVE and HA, and a similar trend was followed by CSVE/HA/DTPA NP and CSVE/HA/DTPA/Cmab NP. The characteristic peaks of crystalline CBT were masked by CSVE and HA, indicating complete encapsulation of drug in prepared nanoparticles.

The X-Ray diffraction pattern (**Figure 5.7)** of CBT revealed crystalline nature and were similar to previously reported peaks [210]. The X-Ray diffraction pattern (Fig. 2B) for CBT showed characteristic peaks at 2θ = 7.787˚, 8.873˚, 10.142˚, 12.595˚, 14.326˚, 15.386˚, 17.708˚, 18.573˚, 21.957 ˚, 23.371˚, 26.994˚, and 33.470˚. The XRD spectra of CBT revealed crystalline nature of pure hydrophobic drug and were similar to previously reported peaks [210]. TPGS revealed two peaks of a high intensity at 18.975˚ and 23.323˚ while CSVE had an amorphous halo diffraction pattern with very small intensity peaks. CSVE/HA NP had only two peaks of lower intensity corresponding to TPGS (19.607˚ and 23.742˚). CSVE/HA/DTPA NP exhibited four peaks corresponding to TPGS (19.582˚ and 23.847˚) and DTPA (32.102˚ and 45.838˚). Whereas, reduction in peak intensity in CSVE/HA/DTPA/Cmab NP for DTPA and TPGS may be due to the surface conjugation of Cmab. The crystalline peaks of CBT were absent in all nanoparticles, probably due to peak dominating effect of amorphous polymer CSVE/HA used for nanoparticle preparation.

DSC Thermogram (**Figure 5.8)** for CBT showed a sharp endothermic peak which was absent in nanoparticles. CSVE and HA had no endothermic peak due to amorphous nature. The signature exothermic peak at 228 ℃ was observed for HA. The TPGS exhibited the characteristic endotherm at 40 ℃. While, CSVE/HA NP, CSVE/HA/DTPA, and CSVE/HA/DTPA/Cmab exhibited characteristic peak of TPGS at 36 ℃, 31 ℃, and 30℃, respectively. The slight shifting of TPGS peak can be due to change in particle size.

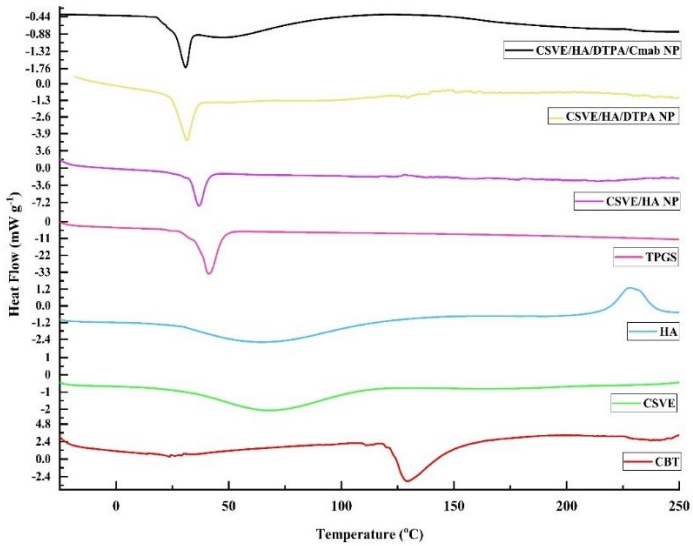

Figure 5.8 The DSC spectra of CBT, CSVE, TPGS, HA, CSVE/HA NP, CSVE/HA/DTPA NP and CSVE/HA/DTPA/Cmab NP.

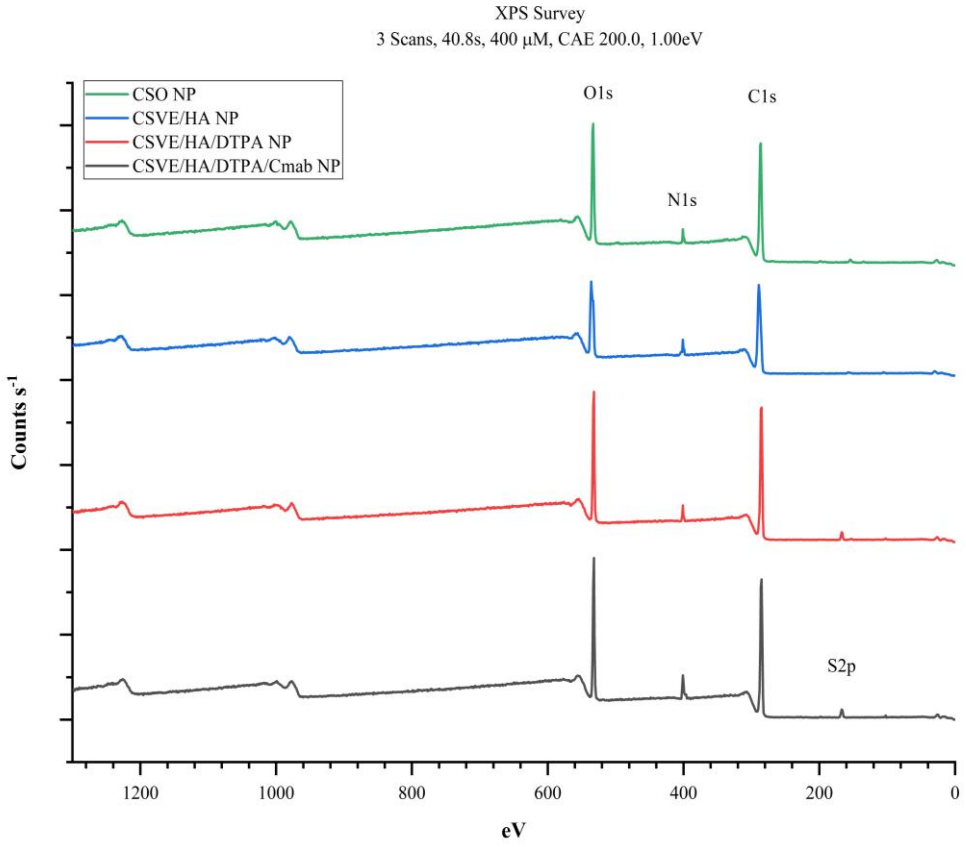

Figure 5.9 The XPS spectra of CSO/HA NP, CSVE/HA NP, CSVE/HA/DTPA NP and CSVE/HA/DTPA/Cmab NP.

The XPS spectra of CSO/HA NP and CSVE/HA NP showed signature C1s, N1s, and O1s peaks as shown in **Figure 5.9.** The XPS spectra of CSO/HA NP and CSVE/HA NP showed signature C1s, N1s, and O1s peaks as shown in Fig. 2D. The atomic percentages of C1s, O1s, and N1s in CSO/HA NP were 68.27%, 25.68% and 6.45% respectively, while CSVE/HA NP yielded atomic percentages of 67.14%, 26.48%, and 6.38% for C1s, O1s, and N1s, respectively. The increase in atomic percentage of O1s may be due to the conjugation of Vitamin E succinate on the CSO backbone. The elemental ratio in CSVE/HA/DTPA NP of 66.11%, 26.82%, and 5.77% for C1s, O1s, and N1s again showed a slight increase in O1s proportion indicating the crosslinking of CSVE by DTPA. This result was further validated due to the presence of 1.3% S2p in the atomic percentages. The proportion of C1s, O1s, N1s, and S2p in CSVE/HA/DTPA/Cmab NP was 64.52%, 23.39%, 9.44%, and 2.65% respectively. A marked increase in N1s and S2p signals indicate the successful conjugation of Cmab on the surface of CSVE/HA/DTPA/Cmab NP. The Cmab is a monoclonal antibody, therefore the amino acids in its sequence results in enhanced signals of N1s and S2p.

5.3.3 Drug release Study

The release study was conducted at conditions corresponding to the systemic circulation (pH 7.4), acidic tumor microenvironment (pH 5.5), and intracellular elevated ROS and reduced pH conditions (pH 5.5+GSH). The redox responsive CSVE/HA/DTPA NP and CSVE/HA/DTPA/Cmab NP showed marked increase in drug release in presence of low pH and glutathione (GSH). Similar results were observed for a redox responsive nanoparticle prepared using DTPA due to cleavage by glutathione (GSH) [193].

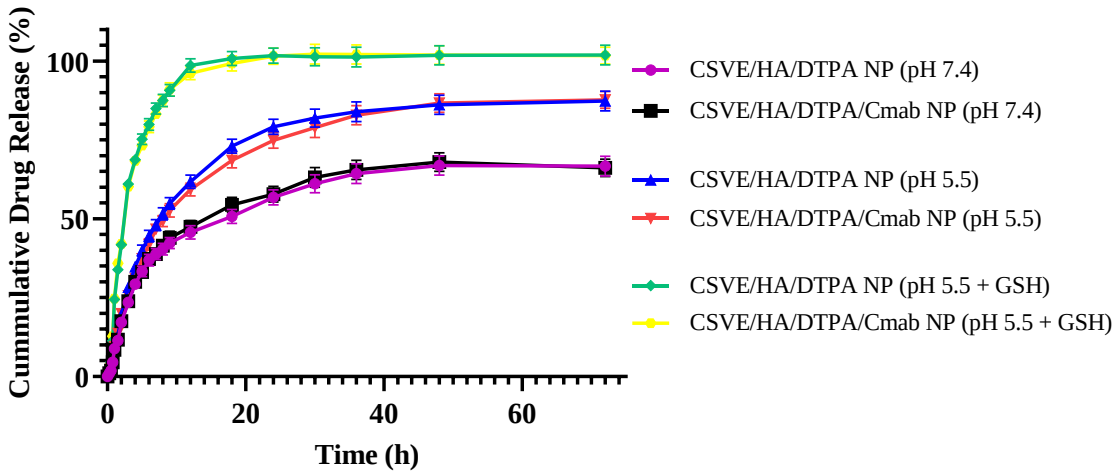

Figure 5.10 Drug release profile of CSVE/HA/DTPA NP and CSVE/HA/DTPA/Cmab NP in pH 7.4 phosphate buffer saline, pH 5.5 acetate buffer, and pH 5.5 acetate buffer and Glutathione (10 mM).

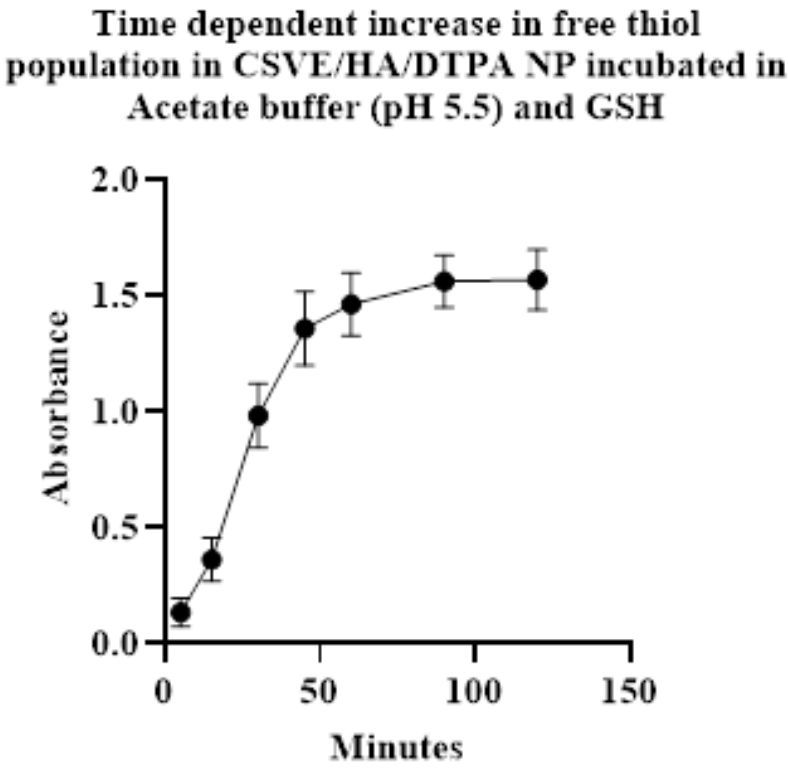

Figure 5.11 Time-dependent change in free thiol concentration in CSVE/HA/DTPA NP suspension after incubation with Acetate buffer (pH 5.5) and GSH

The release rate was highest in pH 5.5 + GSH (10mM) followed by pH 5.5 and pH 7.4. Also, T_{50} for CSVE/HA/DTPA/Cmab NP at pH 7.4, pH 5.5 and pH 5.5+GSH were 15h, 8.5h, and 2.5 h, respectively, exhibiting a similar trend to CSVE/HA/DTPA NP (**Figure 5.10**).

The pH-responsive trend in the release behavior of all the particles can be attributed to protonation of the amino groups on CS at lower pH value responsible for enhanced electrostatic repulsion and thus easy diffusion of loaded drug from NPs [114,211]. However, the increased release of drug in the media comprising low pH and GSH is due to the cleavage of disulfide bonds of the crosslinker DTPA in response to GSH [161,162,183]. The GSH-responsive cleavage of disulfide linkage was further confirmed by Ellman's reagent that showed a rapid release of free thiol group in CSVE/HA/DTPA NP in first 90 min when exposed to Acetate buffer (pH 5.5) + GSH. In the presence of GSH, the disulfide linkage of the crosslinker (DTPA) is cleaved to release free thiol groups that will bind to Ellman's Reagent to give yellow color. The absorbance intensity at 412nm is a direct indicative of the amount of free thiol group. The graph below shows time dependent increase in free thiol groups in CSVE/HA/DTPA incubated in GSH enriched media for 60 min and then becomes constant (**Figure 5.11).** When the CSVE/HA/DTPA NP was exposed to Acetate buffer (pH 5.5) + GSH the disulfide link of DTPA cleaves to release free thiol group, resulting disassembly of the crosslinked polysaccharide nanoparticle consequently increasing the rate of cabazitaxel release.

The drug release kinetic modelling was also done for CSVE/HA/DTPA/Cmab NP that followed Weibull/Gompertz at pH 7.4, Logistic/Probit at pH 5.5 and Weibull/Logistic at pH 5.5+GSH (**Table 5.2** R-square values for mathematical models to determine the goodness of fit.). This suggested controlled drug release via slow drug diffusion mechanism from spherical particles at pH 7.4 [141,142]. At pH 5.5, an initial faster

release followed controlled drug release via diffusion mechanism was observed [212,213]. This could be due to pH responsiveness of prepared nanoparticles that resulted in an initial faster release of drug from nanoparticle surface directly exposed to media followed by controlled release via drug diffusion from core to outer surface and then to media. While at pH 5.5+GSH, the release was faster via erosion and diffusion mechanism as response to GSH responsible for breakage of linkage, loosening of nanoparticle assembly and subsequent dissolution of matrix and drug [140,212].

5.3.3.1 Assessment of storage stability of the prepared nanoparticles

Prepared nanoparticles were also investigated for storage stability. A slight changes in particle size (hydrodynamic diameter), polydispersity index, zeta potential, and entrapment efficiency were observed. However, the differences were non-significant and thus prepared nanoparticles were stable during their storage, suggesting their suitability for long term use. The hydrodynamic size, zeta potential, PDI, and entrapment efficiency of CSVE/HA/DTPA NP and CSVE/HA/DTPA/Cmab did not show any significant (p value > 0.9) change even after storage for 180 days (**Figure 5.12**).

The non-significant change in these characteristics may be attributed to the hydrophilic surface of the nanoparticles due to the presence of pegylated chain on the surface of nanoparticles, hyaluronic acid (a hydrophilic polysaccharide), and cetuximab (in case of CSVE/HA/DTPA/Cmab NP). The hydrophilic environment around the nanoparticle corona ensures optimal hydration on nanoparticles while resuspension resulting in the formation of monodispersed nanosuspension. In case of entrapment efficiency, this insignificant change indicate that the nanoparticles do not show any drug leaking from the nanocarrier due to lyophilization and storage, suggesting the formation of a stable carrier system for lipophilic drugs like cabazitaxel.

Table 5.2 R-square values for mathematical models to determine the goodness of fit.

	CSVE/HA/DTPA NP (pH 7.4)	**CSVE/HA/DTPA/Cmab NP (pH 7.4)**	**CSVE/HA/DTPA NP (pH 5.5)**	**CSVE/HA/DTPA/Cmab NP (pH 5.5)**	**CSVE/HA/DTPA NP (pH 5.5 + GSH)**	**CSVE/HA/DTPA/Cmab NP (pH 5.5 + GSH)**
Hixson-Crowell	0.6139	0.6267	0.8913	0.8988	0.4209	0.4285
Hopfenberg	0.7248	0.7356	0.9591	0.9556	0.9933	0.9933
Baker-Lonsdale	0.9331	0.9271	0.9557	0.9634	0.5597	0.5715
Makoid-banakar	0.9799	0.9827	0.9866	0.9885	0.9405	0.9453
Quadratic	0.7592	0.7663	0.8154	0.8352	0.3343	0.3438
Weibull	**0.9885 β= 0.419**	**0.9860 β= 0.421**	0.9944	0.9967	**0.9979 β= 0.850**	**0.9982 β= 0.805**
Logistic	0.9947	0.9941	**0.9985 β= 2.773**	**0.9986 β= 2.588**	**0.9973 β= 3.521**	**0.9972 β= 3.364**
Gompertz	**0.9950 β= 1.051**	**0.9962 β= 1.082**	0.9959	0.9950	0.9901	0.9901
Probit	0.9834	0.9813	**0.9971 β= 1.490**	**0.9985 β= 1.450**	0.9968	0.9967
Higuchi	0.8626	0.8507	0.8729	0.8996	0.5148	0.5244
First Order	0.7249	0.7358	0.9591	0.9556	0.9930	0.9934
Zero order	0.1487	0.1248	0.2259	0.2956	-0.6505	-0.6481
Peppas and Sahlin	0.9792	0.9810	0.9831	0.9864	0.9329	0.9389
Korsmeyer Peppas	0.9816	0.9836	0.9865	0.9715	0.9749	0.9690

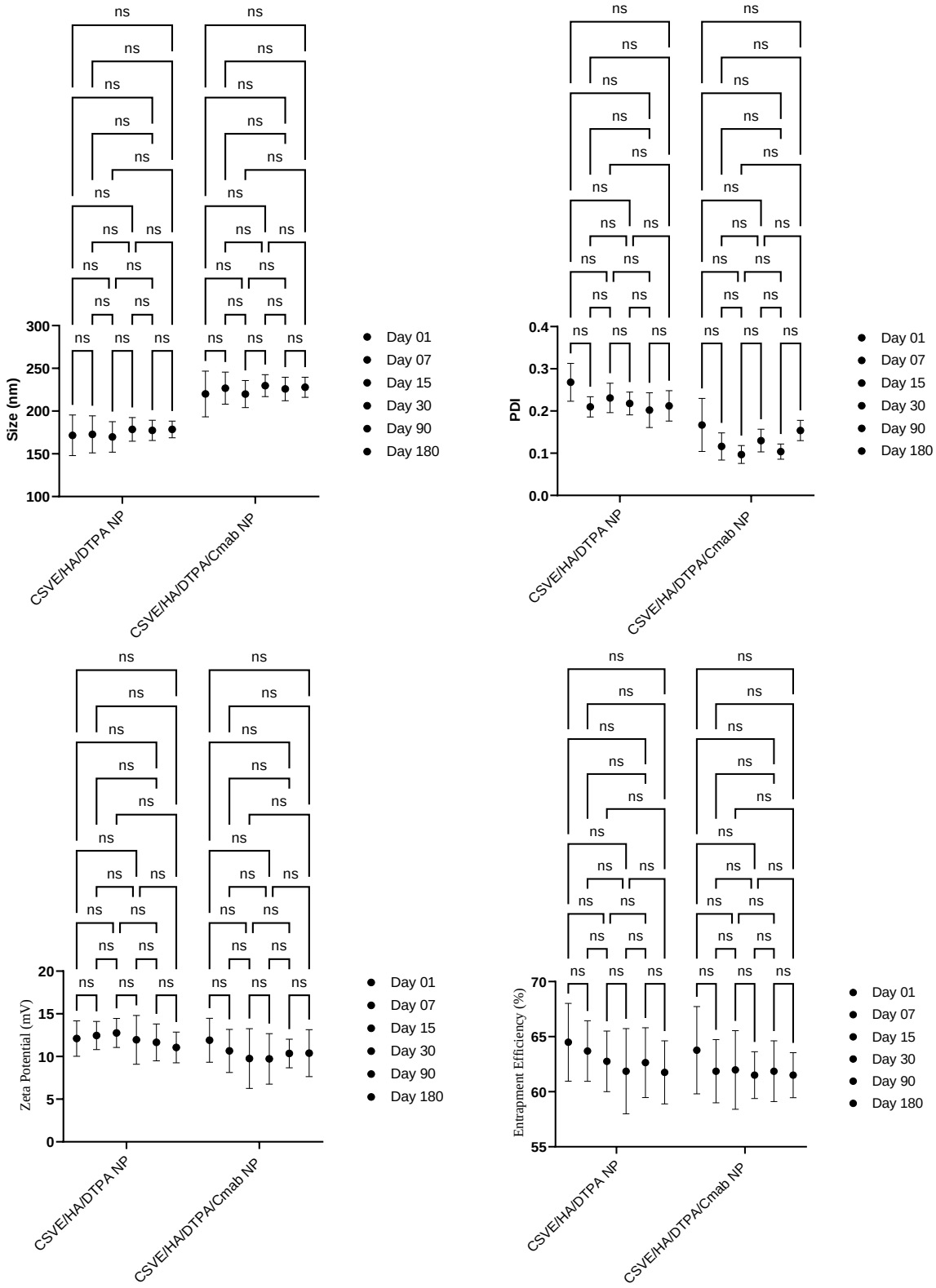

Figure 5.12 Effect of the storage of Lyophilized nanoparticles on Hydrodynamic size, PDI, Zeta Potential, and Entrapment Efficiency Data presented as Mean ± SD (vertical bars); n=6. ns (p-value > 0.05)

5.3.4 In vitro Study

5.3.4.1 Cell Viability Assay

To investigate the cytotoxicity and antiproliferative activity of the formulations, MDA-MB-231, T47D, and HCT116 cells were exposed to various concentrations for 24 h and their IC_{50} values were determined. The formulations; CSO/HA NP, CSVE/HA NP, CSVE/HA/DTPA NP, and CSVE/HA/DTPA/Cmab NP induced significant concentration-dependent inhibition on the MDA-MB-231 cell line (**Figure 5.13**).

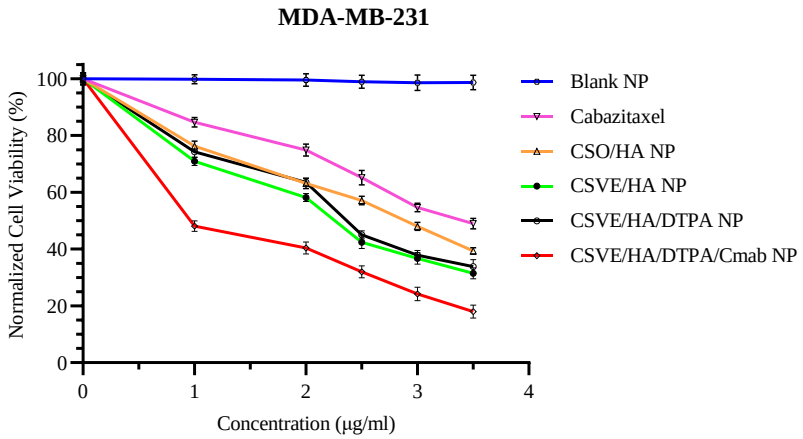

Figure 5.13 *In vitro* cell viability of MDA-MB-231 cells after treatment with Cabazitaxel-loaded formulations for 24 h. Data presented as Mean ± SD (vertical bars); n=6.

MTT data revealed that formulations exhibit a substantial suppressive effect on the proliferation of the MDA-MB-231 cell line. The CSO/HA NP showed an IC_{50} value of 2.816 ± 0.182 µg/ml, which was a 1.25-fold reduction compared to cabazitaxel (3.521 ± 0.294 µg/ml). Also, the IC_{50} value of non-targeted redox responsive CSVE/HA/DTPA NP and CSVE/HA NP was found to be 2.105 ± 0.133 µg/ml and 2.358 ± 0.167 µg/ml, respectively. However, CSVE/HA/DTPA/Cmab NP elicited the highest inhibitory effect, showing IC_{50} value at 1.04 ± 0.185 µg/ml concentration in MDA-MB-231 cells. This could be attributed to increased internalization of CSVE/HA/DTPA/Cmab NP via

receptor-mediated endocytosis. To confirm this, cellular uptake study was conducted in MDA-MB-231 cells.

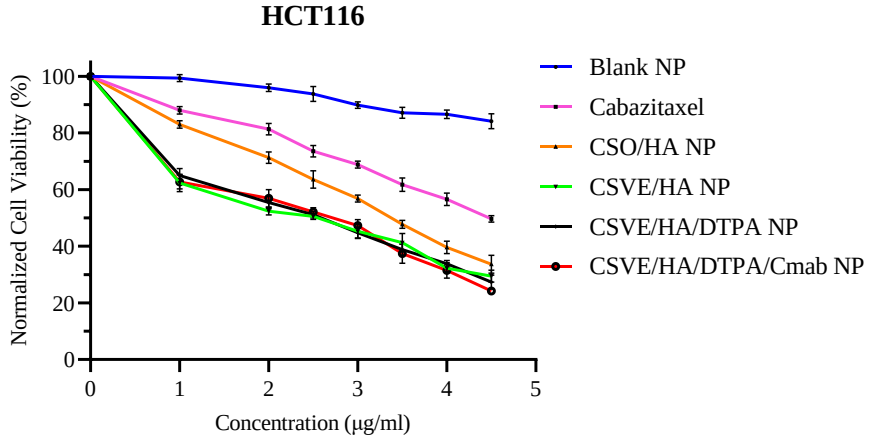

Figure 5.14 *In vitro* cell viability of HCT116 cells after treatment with Cabazitaxel-loaded formulations for 24 h. Data presented as Mean ± SD (vertical bars); n=6.

When HCT116 cells were treated with various concentrations of the prepared formulations for 24 hours, a concentration dependent decline in cell viability was observed with all the Cabazitaxel loaded formulation and Cabazitaxel. The observed IC_{50} for Cabazitaxel, CSO/HA NP, CSVE/HA NP, CSVE/HA/DTPA NP, and CSVE/HA/DTPA/Cmab NP was found to be 5.924 ± 0.724 µg/ml, 3.490 ± 0.283 µg/ml, 2.167 ± 0.171 µg/ml, 2.205 ± 0.102 µg/ml, 2.158 ± 0.159 µg/ml respectively (normalized cell viability versus time graph in **Figure 5.14**). The results show a significant decline in IC_{50} of CSVE based nanoparticles, but surface conjugation with Cetuximab did not yield any significant reduction in IC_{50}.

Similar observations were made when the T47D cells were treated with the prepared nanoparticles. The groups exposed to varying concentrations of Cabazitaxel, CSO/HA NP, CSVE/HA NP, CSVE/HA/DTPA NP, and CSVE/HA/DTPA/Cmab NP the IC_{50} was found to be 6.675 ± 0.502 µg/ml, 5.651 ± 0.318 µg/ml, 3.043 ± 0.186 µg/ml, 3.195 ± 0.295

µg/ml, and 2.849 ± 0.143 µg/ml, respectively (normalized cell viability versus time graph in **Figure 5.15**). The non-significant difference in the IC_{50} value of CSVE/HA/DTPA NP and CSVE/HA/DTPA/Cmab NP treated groups may be attributed to lower expression of EGFR on the surface of these cell line which is highly expressed on MDA-MB-231 indicating the possible selectivity of CSVE/HA/DTPA/Cmab NP towards the cells over expressing EGFR. This observation was further confirmed by assessing the effect of EGFR-blocking on the cellular uptake of CSVE/HA/DTPA/Cmab NP in MDA-MB-231 cells.

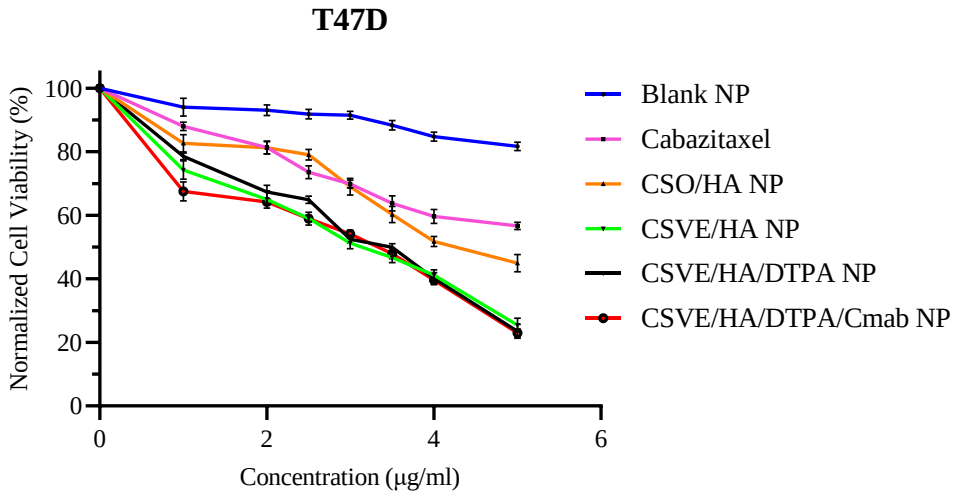

Figure 5.15 *In vitro* cell viability of T47D cells after treatment with Cabazitaxel-loaded formulations for 24 h (n=6).

5.3.4.2 Cellular uptake Study

Fluorescence microscopic showed higher cellular internalization potential of CSVE/HA NP than CSO/HA NP. This could be attributed to VES conjugation on CSO backbone that render amphiphilic character to the conjugate (CSVE) and thereby improving cellular localization via P-gp inhibition. Similar results were observed for DOX loaded chitosan-g-TPGS NP compared to only Chitosan NPs [114].

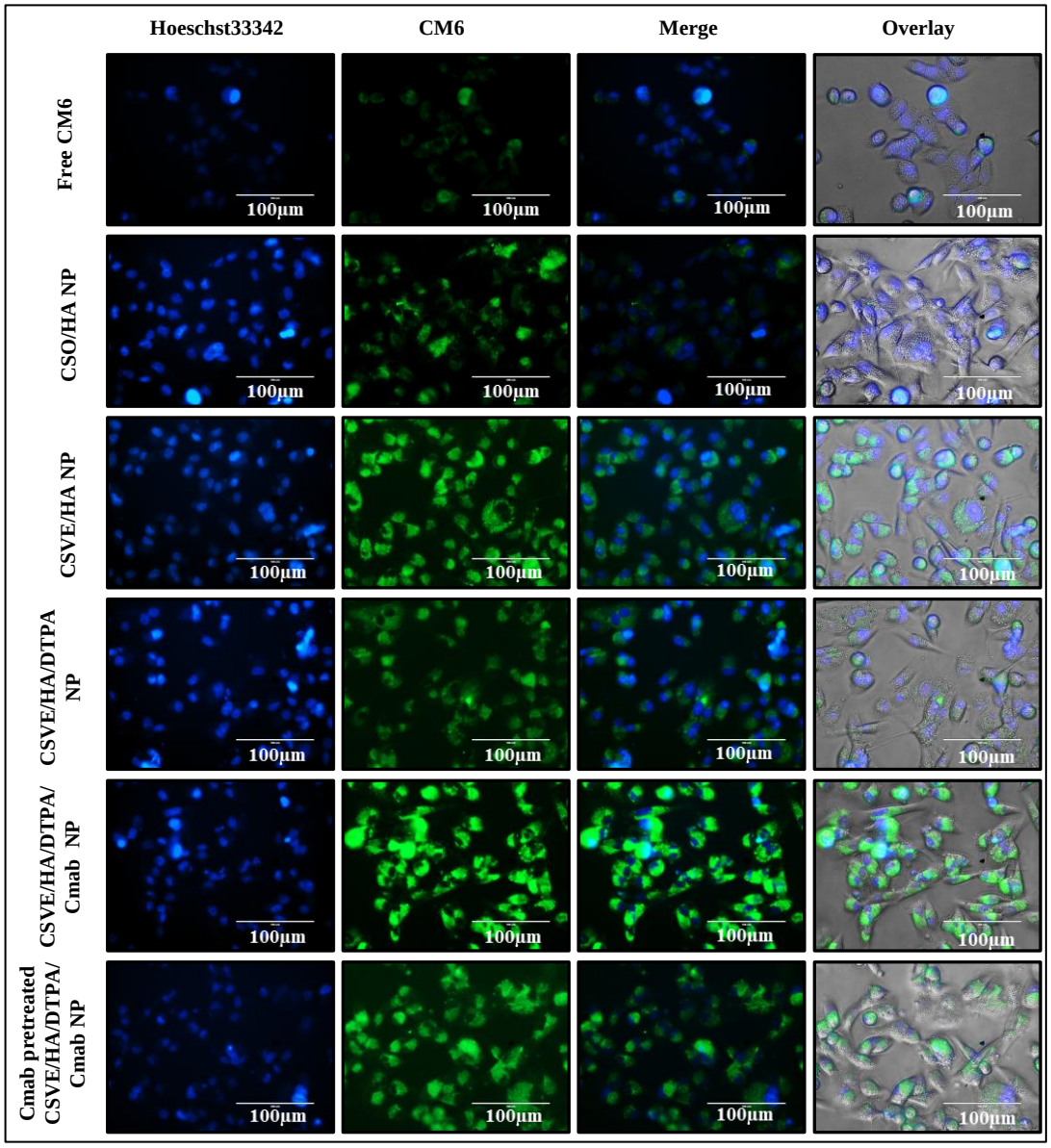

Figure 5.16 Fluorescence microscopy images of MDA-MB-231 cells after 6 h incubation with the fluorescent CM6-loaded formulations. The blue fluorescence from DAPI channels shows Hoechst 33342 stained nuclei while the third column shows an overlay image of Hoechst and GFP. The fourth column represents an overlay image of phase contrast, GFP, and Hoechst 33342. Each scale bar represents 100 µm. GFP channel showing higher level of green fluorescence in CM6 loaded CSVE/HA/DTPA/Cmab NP treated cells compared to free CM6 and CM6-loaded CSVE/HA/DTPA NP treated cells due to receptor-mediated cellular uptake of CM6 in the cytoplasm. The CM6-loaded

CSVE/HA NP also exhibited superior intracellular localization of CM6 compared to CM6-loaded CSO/HA NP which may be attributed to the amphiphilic nature of the CSVE conjugate. The Cmab pretreated cells exhibited reduced uptake of CM6 which may be due to the competitive binding of Cmab to the EGFR.

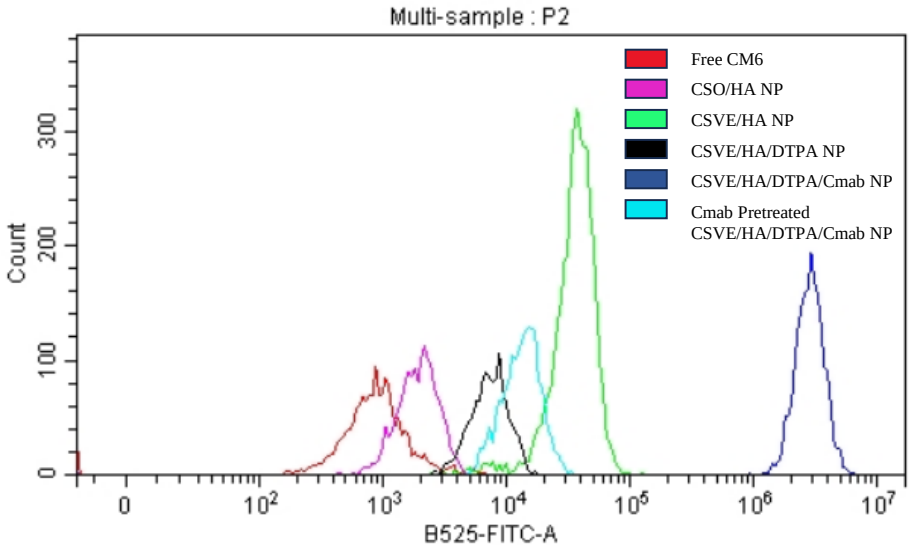

Figure 5.17 Quantitative assessment of intracellular uptake of green fluorescent CM6 in MDA-MB-231 cells treated with free CM6, CSO/HA NP, CSVE/HA NP, CSVE/HA/DTPA NP, CSVE/HA/DTPA/Cmab NP, Cmab pre-treated CSVE/HA/DTPA/Cmab NP at 0.2 µg ml^{-1} concentrations of CM6 for 6 h using flow cytometry. The blue peak shows the highest cellular uptake of CM6 in CM6-loaded CSVE/HA/DTPA/Cmab NP treated cells compared to free CM6, CSO/HA NP, CSVE/HA NP, CSVE/HA/DTPA NP, and CSVE/HA/DTPA/Cmab NP treated cells.

Furthermore, CSVE/HA/DTPA NP obtained on crosslinking of CSVE/HA NP, had slightly lower cellular uptake compared to CSVE/HA NP, but still higher than CSO/HA NP (**Figure 5.16**). This could be due to deformable structure of CSVE/HA NP that may have assisted in cellular internalization. In addition, CSVE/HA/DTPA/Cmab exhibited highest cellular uptake in MDA-MB-231 cells, showing maximum emission of green fluorescence

in the cytoplasmic region than free CM6, CSO/HA NP, CSVE/HA NP, and CSVE/HA/DTPA NP.

The higher cellular internalization was attributed to conjugated cetuximab directed uptake in MDA-MB-231 cells. The blocking study was further conducted to confirm the role of cetuximab in assisting targeted cellular internalization of nanoparticles. The study indicated diminished uptake upon pretreatment of cells with cetuximab leading to competitive binding of the antibody to EGFR causing hindrance in receptor-mediated endocytosis of CSVE/HA/DTPA/Cmab NP. Further, the quantitative analysis performed using flow cytometry yielded results that concurred with the above findings (**Figure 5.17**).

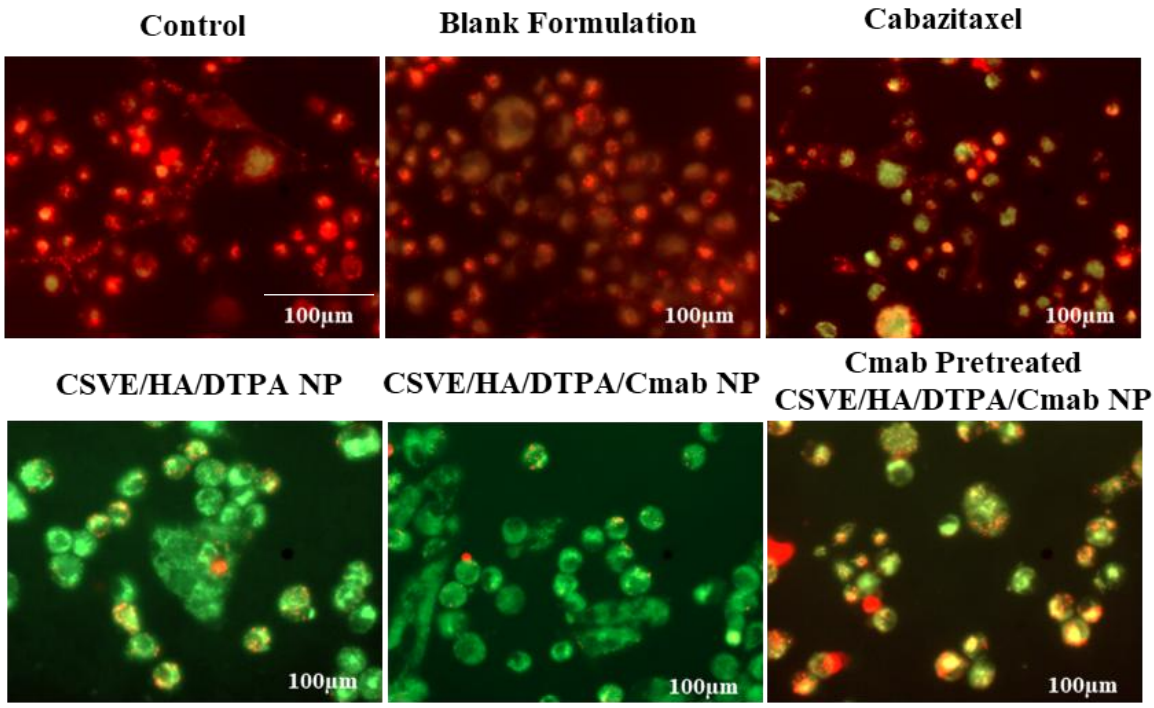

Figure 5.18 Assessment of mitochondrial membrane potential by JC-1 dye in control and treated MDA-MB-231 cells after treatment with Cabazitaxel, CSVE/HA/DTPA NP, CSVE/HA/DTPA/Cmab NP, and Cmab pretreated CSVE/HA/DTPA/Cmab NP. The CSVE/HA/DTPA/Cmab NP treated group showed maximum depolarization (green fluorescence of JC-1 monomer) in cells. In contrast, the control group exhibited an

accumulation of JC-1 monomers in negatively charged and energized normal mitochondria to spontaneously form J aggregates (Red fluorescence).

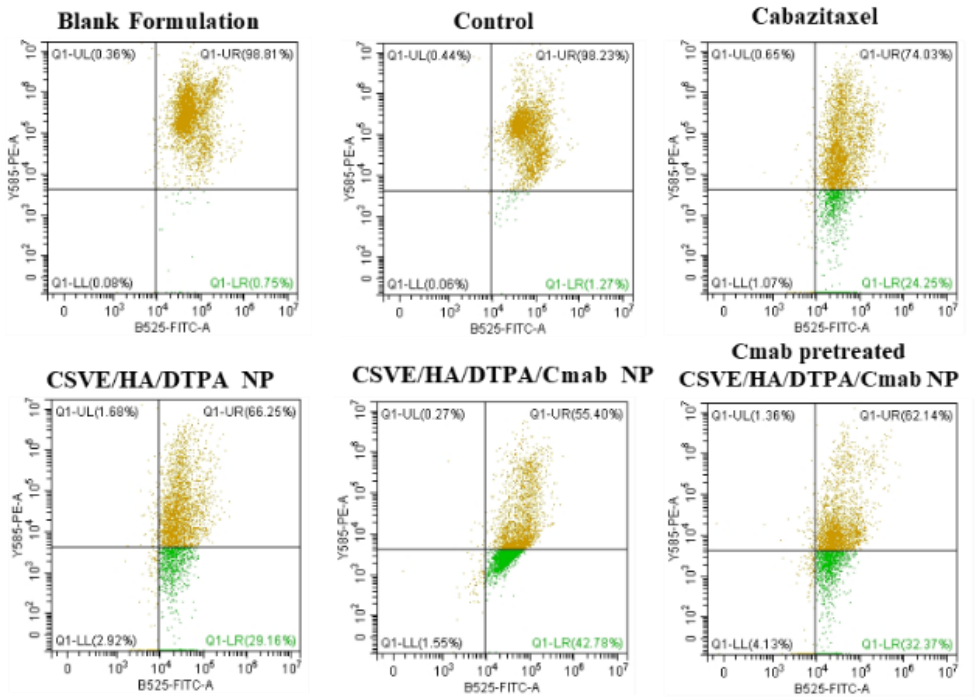

Figure 5.19 Quantitative detection of mitochondrial membrane potential in MDA-MB-231 after treatment with the formulations through flow cytometry. The upper right and lower right quadrants represent cells with normal mitochondrial membrane potential and depolarized mitochondria respectively.

5.3.4.3 Mitochondrial membrane potential

Taxanes are reported to evoke a rapid decline in mitochondrial membrane potential. Microscopic evaluation for the detection of J-aggregates and J-monomers in MDA-MB-231 cells after treatment with the formulations indicated significantly effect on mitochondrial membrane potential. As seen in **Figure 5.18**, J-aggregates (distributed red fluorescence in the cytoplasmic region) were seen control and blank formulation treated groups, indicating no alteration in mitochondrial membrane potential. The J-monomers (green fluorescent signals) were increasingly seen in the cabazitaxel and CSVE/HA/DTPA NP treated groups due to significant mitochondrial depolarization. However,

CSVE/HA/DTPA/Cmab NP treated group exhibited maximum J-monomer formation. Also, the blocking study showed a marked reduction in the J-monomer formation. The data conforms with the cellular uptake studies, indicating the receptor mediated endocytosis of CSVE/HA/DTPA/Cmab NP results in superior anti-proliferative effect on MDA-MB-231 cell line. Further, the mitochondrial membrane potential was also validated through the flow cytometry, also indicated a similar trend (**Figure 5.19**). In brief, 41.335 % cell population were showed decreased mitochondrial membrane potential in CSVE/HA/DTPA/Cmab NP treated group, which was significantly higher (P value < 0.001) than 33.665 % in CSVE/HA/DTPA NP. In comparison, control cells showed 0.95 % cell populations with decreased mitochondrial membrane potential.

5.3.4.4 Study of mitochondrial distribution pattern

Mitochondria are the cell's powerhouse and produce ATP through oxidative phosphorylation which controls a variety of physiological activities in cells, the pro-apoptotic signal of the cells can strongly correlate with mitochondrial dynamics and, therefore impacts its distribution pattern. According to several findings, cytotoxic materials that cause apoptosis can influence the mitochondrial distribution pattern. The distribution pattern of mitochondria in MDA-MB-231 cells stained with MitoTracker™ Red is shown in the microscopic image (**Figure 5.20**). Aggregation of mitochondria causes mitochondrial dysfunction, a positive regulator of apoptosis. The control treatment cells have consistent red fluorescence and uniform distribution of mitochondria throughout the cytoplasm. MDA-MB-231 treated with 1µg ml^{-1} concentration of formulations induced aggregation of mitochondria towards perinuclear space and generated bright red fluorescence, indicating the involvement of an intrinsic mitochondrial pathway in apoptosis. The aggregation of mitochondrial was significant in CSVE/HA/DTPA NP and CSVE/HA/DTPA/Cmab NP treated groups compared to control and CBT treated groups,

with CSVE/HA/DTPA/Cmab NP treated group exhibiting maximum aggregation. The Cmab pretreated group showed reduction in mitochondrial aggregation indicating the role of EGFR in receptor mediated endocytosis of CSVE/HA/DTPA/Cmab NP.

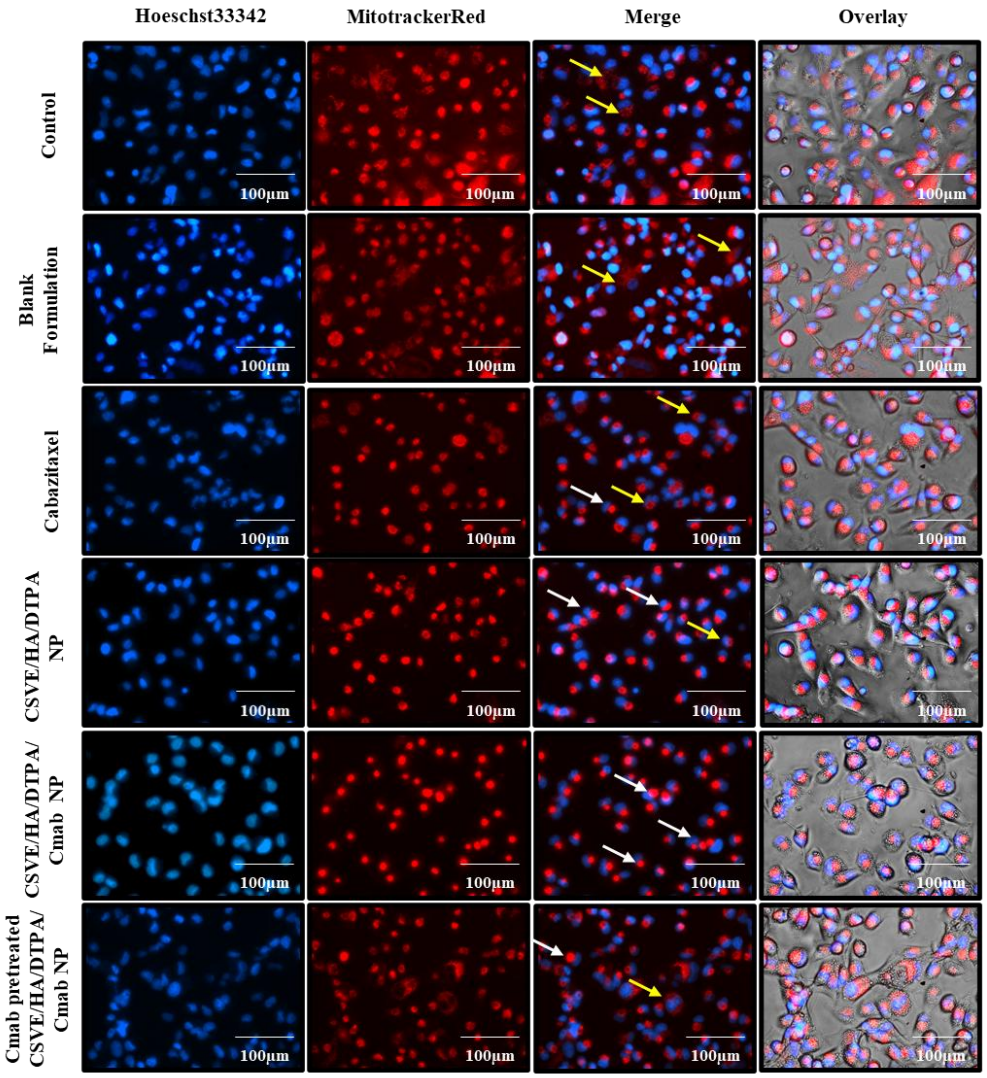

Figure 5.20 Pattern of mitochondrial distribution in MDA-MB-231 cells using Mitotracker™ Red after treatment with Cabazitaxel, CSVE/HA/DTPA NP, CSVE/HA/DTPA/Cmab NP, and Cmab pretreated CSVE/HA/DTPA/Cmab NP. The uniform distribution of mitochondria was seen in control cells represented by the yellow arrow while aggregated mitochondria were observed in the treatment group represented by the white arrows. The CSVE/HA/DTPA/Cmab treated cells showed the highest mitochondrial aggregation.

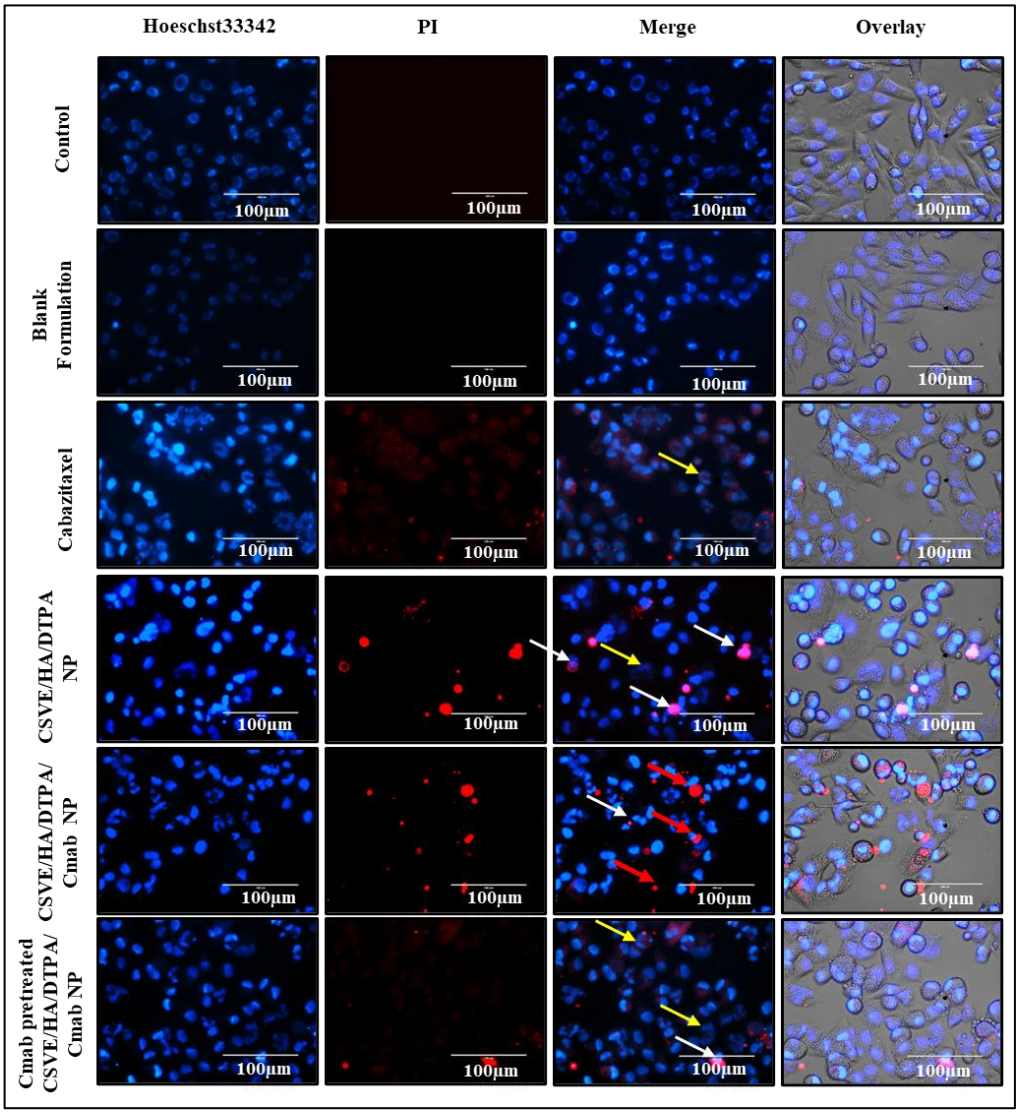

Figure 5.21 Combined images of Hoechst33342/PI-stained MDA-MB-231 cells after treatment with the formulations. The yellow, white, and red arrows represent early apoptotic, late apoptotic, and necrotic cells. Cells emitting blue fluorescence are Hoechst positive while those with red fluorescence are PI positive.

5.3.4.5 Qualitative assessment of apoptosis

Hoechst33342 dye was used to observe the nuclear morphology of MDA-MB-231 cells treated with various formulations (**Figure 5.21**). After treatment with Hoechst33342 dye, the live cells usually emit blue fluorescence. Hoechst33342 mainly stains the chromatin present in cells. The apoptotic cells give a brighter blue fluorescence due to condensed

nature of chromatin compared to normal cells. On the other hand, PI is a DNA binding dye that only permeant to dead cells and stain the cells only in case of loss of plasma membrane integrity.

In case of control and blank formulation, only a low-bright blue fluorescence was observed denoting live cells with highly integrated plasma membrane. While for CBT treatment groups, a brighter blue and red fluorescence was observed indicative of highly condensed nucleus and presence of apoptotic and necrosis cells. Brighter blue fluorescence of Hoechst33342 and red fluorescence of PI in CSVE/HA/DTPA NP and CSVE/HA/DTPA/Cmab NP treated group revealed presence of fragmented chromatin and loss of plasma membrane integrity, indicative of late apoptosis and cell death. The brighter fluorescence was representative of higher nuclear condensation and increased number of apoptotic nuclei in nanoparticles treated groups.

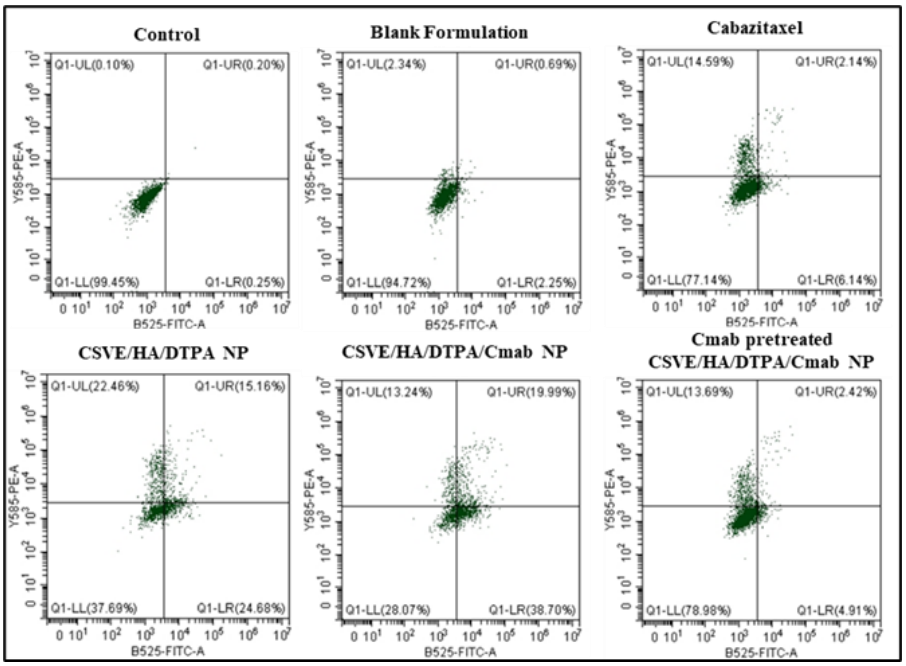

Figure 5.22 Quantitative assessment of apoptosis by AnnexinV/PI dual staining through Flow cytometry in treated MDA-MB-231 cells. AnnexinV/PI dual staining discriminates

the percentage of live (lower left quadrant), early apoptotic (lower right quadrant), late apoptotic (upper right quadrant), and necrotic or dead cells (upper left quadrant).

5.3.4.6 Quantitative analysis of apoptosis

An initial event in apoptosis is detected by the disintegration of phospholipids and an undefined plasma layer. In the apoptotic cells, Annexin V binds to phosphatidylserine exposed on the extracellular layer of plasma membrane which is otherwise located on the intracellular layer in normal cells. The necrotic and late apoptotic cells can also be stained by DNA-binding propidium iodide (PI) which does not penetrate across viable cells. Thus, the AnnexinV- propidium iodide (PI) double labelling assay was used to demonstrate the induction of apoptosis in MDA-MB-231 cells after treatment with the formulations.

As shown in the flow cytometry data analysis (**Figure 5.22** Quantitative assessment of apoptosis by AnnexinV/PI dual staining through Flow cytometry in treated MDA-MB-231 cells. AnnexinV/PI dual staining discriminates the percentage of live (lower left quadrant), early apoptotic (lower right quadrant), late apoptotic (upper right quadrant), and necrotic or dead cells (upper left quadrant).Error! Reference source not found. the lower left quadrant concerns the viable cells (Annexin V−/PI− cells) represent 99.545 % cell population in control group decreases to 30.09 % in the CSVE/HA/DTPA/Cmab NP treated cells. The lower right quadrant comprises early apoptotic cells (Annexin V+/PI−cells) which increased from 0.195 % in the control cells to 38.65 % in CSVE/HA/DTPA/Cmab NP treated cells. Also, the upper right (Annexin V+/PI+) and upper left quadrants (Annexin V–/PI+ cells) represent the late apoptotic cells and dead cells. The control group exhibits 0.17 % and 0.09 % cell population upper right and left quadrants respectively. The CSVE/HA/DTPA/Cmab NP-treated group showed 18.56 % and 12.7 % cell populations in the upper left and right quadrants respectively. Although the dead cell population in CSVE/HA/DTPA NP treated group was higher than the

CSVE/HA/DTPA/Cmab NP treated group, the overall apoptotic and dead cell population was significantly (P value < 0.001) higher in later.

5.3.5 In vivo Studies

5.3.5.1 Pharmacokinetics

The pharmacokinetics studies performed on SD female rats treated with CBT, CSVE/HA/DTPA NP, and CSVE/HA/DTPA/Cmab NP (**Figure 5.23**). Nanoparticles dose was equivalent to 10 mg kg^{-1} CBT administered via. intravenous route through tail vein method. The pharmacokinetic parameters of formulations generated from PKSolver add-in for Excel are mentioned in (**Table 5.3**).

Table 5.3 Pharmacokinetic parameters of various formulations determined from plasma concentration vs time plot

Parameters	**Unit**	**Cabazitaxel**	**CSVE/HA/DTPA NP**	**CSVE/HA/DTPA/Cmab NP**
$t_{1/2}$	h	11.3409	30.7382	38.3640
T_{max}	h	0.25	0.25	0.25
C_{max}	ng/ml	18669.4540	18119.0039	18369.1091
C_0	ng/ml	23473.1886	21774.7884	22217.6985
AUC_{0-t}	ng/ml*h	96771.0839	247526.4187	226707.1421
AUC_{0-inf_obs}	ng/ml*h	103915.5047	358035.5039	369966.0585
$AUMC_{0-inf\_obs}$	$ng/ml*h^2$	1408825.881	14463854.26	18809769.52
MRT_{0-inf_obs}	H	13.5574	40.3978	50.8419
$Cl_{\_obs}$	$(mg\ kg^{-1})/(ng$	9.6232	2.7930	2.7029

	$ml^{-1}) h^{-1}$		
F_{rel}	-	3.44	3.56

A sustained-plasma concentration of CBT was observed in CSVE/HA/DTPA NP, and CSVE/HA/DTPA/Cmab NP treated groups as compared to CBT. The Cmax observed was highest with CBT (18669 ng ml^{-1}) followed by CSVE/HA/DTPA/Cmab NP (18369 ng ml^{-1}) and CSVE/HA/DTPA NP (18119 ng ml^{-1}).

However, area under the curve for CSVE/HA/DTPA NP and CSVE/HA/DTPA/Cmab NP was three to four-fold of CBT. This could be due to higher clearance of CBT from systemic circulation as compared to CSVE/HA/DTPA NP and CSVE/HA/DTPA/Cmab NP. The $t_{1/2}$ of only 11.34 hr was observed for CBT while $t_{1/2}$ for CSVE/HA/DTPA NP and CSVE/HA/DTPA/Cmab NP were 30.74 h and 38.36 h, respectively. The mean retention time (MRT) of drug was also shorter for CBT (13.56 h) than CSVE/HA/DTPA NP (40.40 h) and CSVE/HA/DTPA/Cmab NP (50.84 h). The results indicate that the prepared nanoparticles provided longer systemic circulation than CBT, allowing the sustained drugs concentration to reach the target site and leverage its actions, which could contribute to a better therapeutic response.

5.3.5.2 Biodistribution

Biodistribution study revealed a distinct pattern of higher drug concentration maintained in tumor tissues even after 48 hours of administration of dose (**Figure 5.23**). The groups treated with CSVE/HA/DTPA/Cmab NP showed significantly (p value < 0.001) higher drug permeation in tumor tissues after 2 h of dose administration. The drug concentration in tumor tissue further further increased after 10 h and showed significantly higher levels even at 48 h. The CSVE/HA/DTPA NP also showed better tumor tissue permeation and retention than standard cabazitaxel. The concentration of cabazitaxel in liver also showed

similar trend, indicating that the prepared nanoparticles were able to maintain the systemic concentration of cabazitaxel for longer time. The distribution in lungs however showed similar concentration of cabaziataxel in all the groups at 2h and 10 h, but higher concentration in nanoparticle treated groups at 24 h and 48 h, indicating that sustained systemic levels of cabazitaxel loaded nanoparticles were achieved.

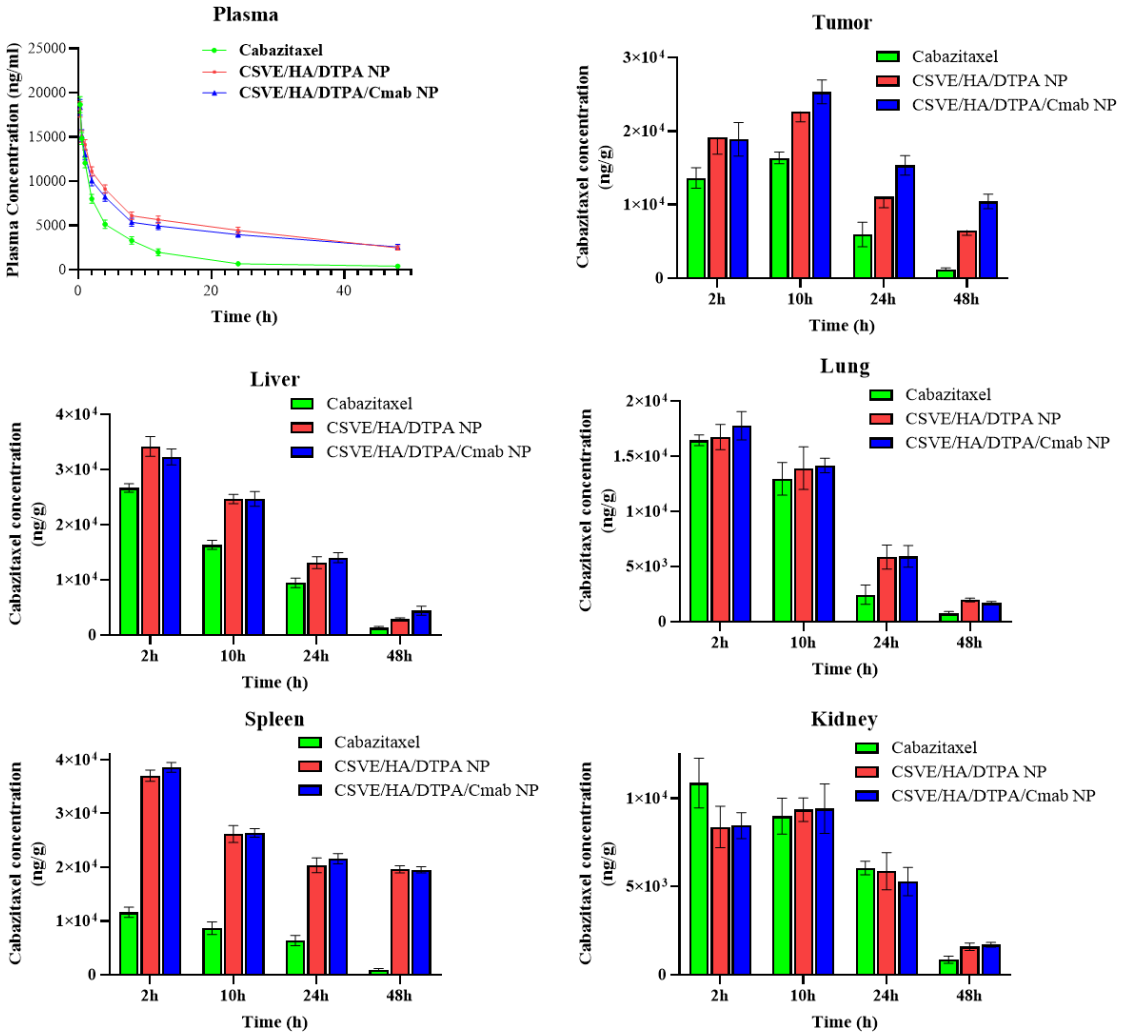

Figure 5.23 Concentration of Cabazitaxel in plasma, tumor, liver, lung, spleen and kidney after intravenous administration of Cabazitaxel, CSVE/HA/DTPA NP, and CSVE/HA/DTPA/Cmab NP. Data presented as Mean ± SD (vertical bars); n=12.

The drug concentration in kidney was similar for all the treatment groups throughout the observation period with nanoparticles showed higher levels only at 48 h, probably due to

the higher systemic levels of cabazitaxel maintained in these groups. The higher splenic concentration in case of CSVE/HA/DTPA NP and CSVE/HA/DTPA/Cmab NP is due to their size. The nanocarriers are trapped in the spleen and results in higher concentration of cabazitaxel in the tissue sample. The results indicate that the nanocarriers are able to maintain the drug concentration in systemic circulation for longer periods and selectively target the tumor tissues.

5.3.5.3 Tumor Regression Analyses

The body weight of all the animals were recorded after each treatment for the complete duration of tumor regression analysis (**Figure 5.24**). The normal SD rats and control (untreated tumor bearing SD rats) groups showed gradual increase in body weight over the period of four weeks of treatment. The body weight of tumor bearing group treated with CBT reduced significantly ($p < 0.0001$) compared to normal and untreated tumor-bearing group. The body weight of group treated with targeted nanoparticles was similar to normal and control group (p=ns). However, change in body weight was significant ($p < 0.0001$) in CBT treated groups compared to non- targeted and targeted. Non-significant change in body weight of targeted nanoparticles indicated reduction in toxicity of CBT due to selective accumulation in cancer cells while, free CBT drug induced significant reduction in body weight indicating systemic toxicity due to non-selective distribution.

Tumor were collected after complete duration of treatment (**Figure 5.25**). The tumor volume significantly increased in untreated tumor-bearing rats while groups treated with nanoparticles showed marked reduction in tumor volume ($p < 0.0001$). The tumor volume reduction was highest in CSVE/HA/DTPA/Cmab NPs followed by CSVE/HA/DTPA NP and CBT treated group. Total tumor volume reduction of CSVE/HA/DTPA/Cmab NP was about 4.57-fold ($p = 0.0057$) and 15.23-fold ($p < 0.0001$) compared to CSVE/HA/DTPA NP and CBT treated groups (**Figure 5.24**).

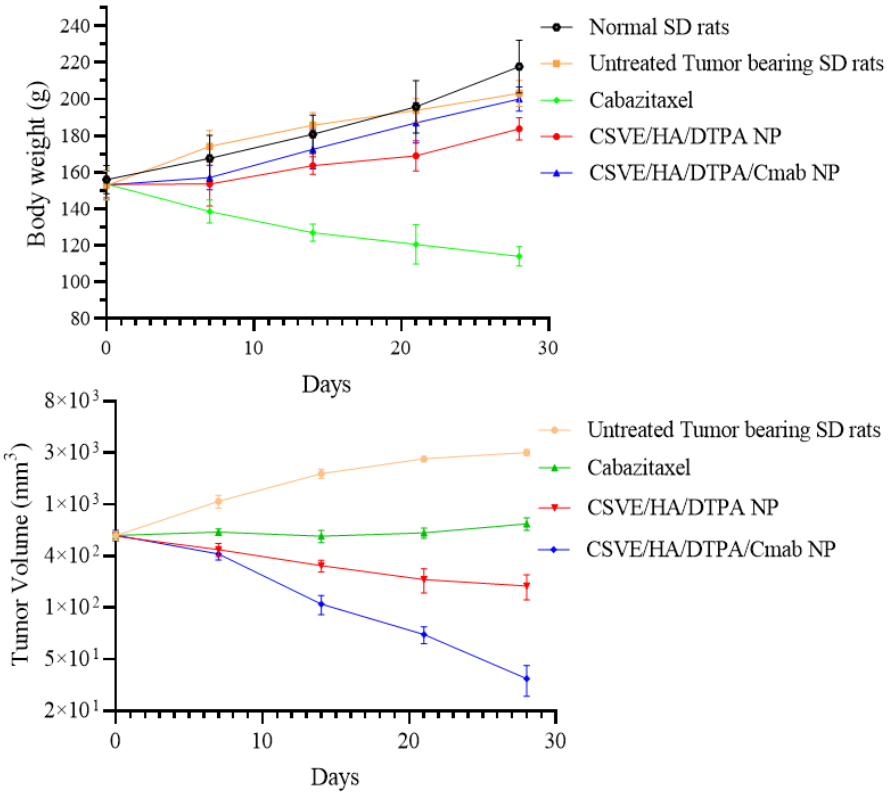

Figure 5.24 Body weight and tumor volume of normal SD rats, tumor-bearing SD rats, and formulation treated tumor-bearing SD rats over the 28 days treatment period. Data presented as Mean ± SD (vertical bars); n=5.

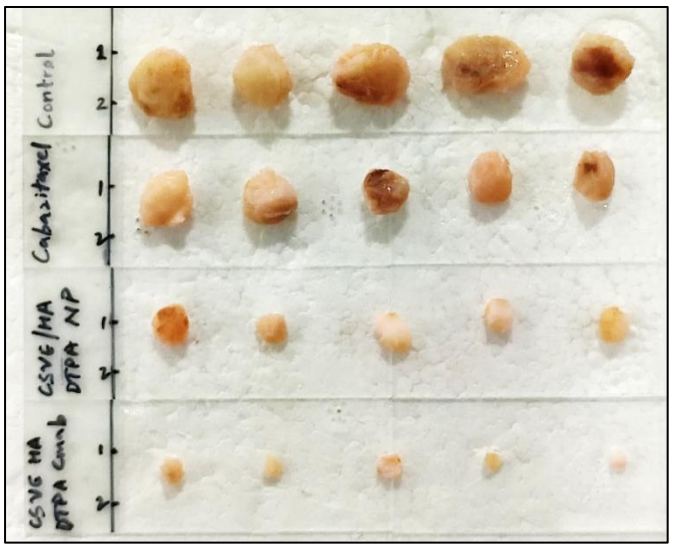

Figure 5.25 Images of the tumors harvested from various treatment groups after end of 28-day treatment period. The line marked on the left side of tumor represents a cm-scale.

5.3.5.4 Survival Analysis

CSVE/HA/DTPA/Cmab NP showed significantly increase in survival rate compared to other groups (**Figure 5.26**). Median survival time of rats was 37, 56, 92 and >120 days in groups treated with Control, CBT, CSVE/HA/DTPA NP, and CSVE/HA/DTPA/Cmab NP. CBT treated group increased the survival by 51% compared to control group while CSVE/HA/DTPA NP, and CSVE/HA/DTPA/Cmab NP showed higher survival by 148% and >230%, respectively. In comparison to CBT and non-targeted nanoparticles treated groups, the survival period for targeted nanoparticles treated was more. This may be attributed to the higher efficiency of prepared nanoparticles to selectively target cancer cells via receptor mediated endocytosis, thereby providing better therapeutic effect.

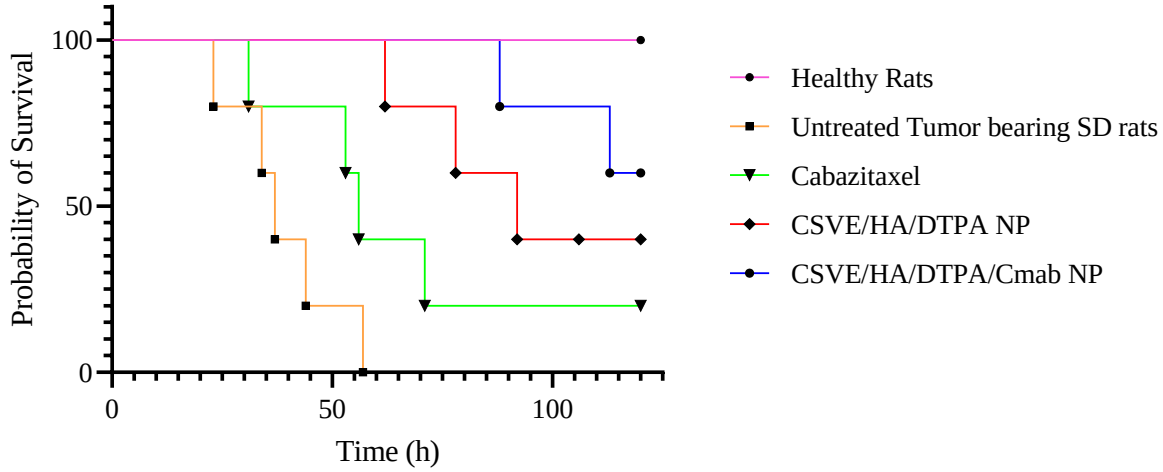

Figure 5.26 Survival rates of tumor-bearing SD rats after treatment with formulations, day 0 represents the day of administration of first dose after the tumor volume reached ~ 500 mm^3.

5.3.5.5 Histopathology Study

The H&E staining was used to determine the histological changes on tumor induction and their treatment with various formulations (**Figure 5.27(A)**). Normal tissue exhibited

normocellular structure i.e. normal arrangement of fat tissue/adipocytes, lobules, & duct with no signs of proliferated cancer cells [143–145]. Whereas, tumor bearing SD rats showed tissue rich in nuclear division showing invasive carcinoma (IC) with cells spread into surrounding stromal tissue (ST), disorganized and loosely connected. The immune cells may also have infiltrated into stromal tissue and several empty spaces occurred in stromal section [146]. The results revealed successful establishment of breast cancer (red arrows indicate cancer cells area) [214].

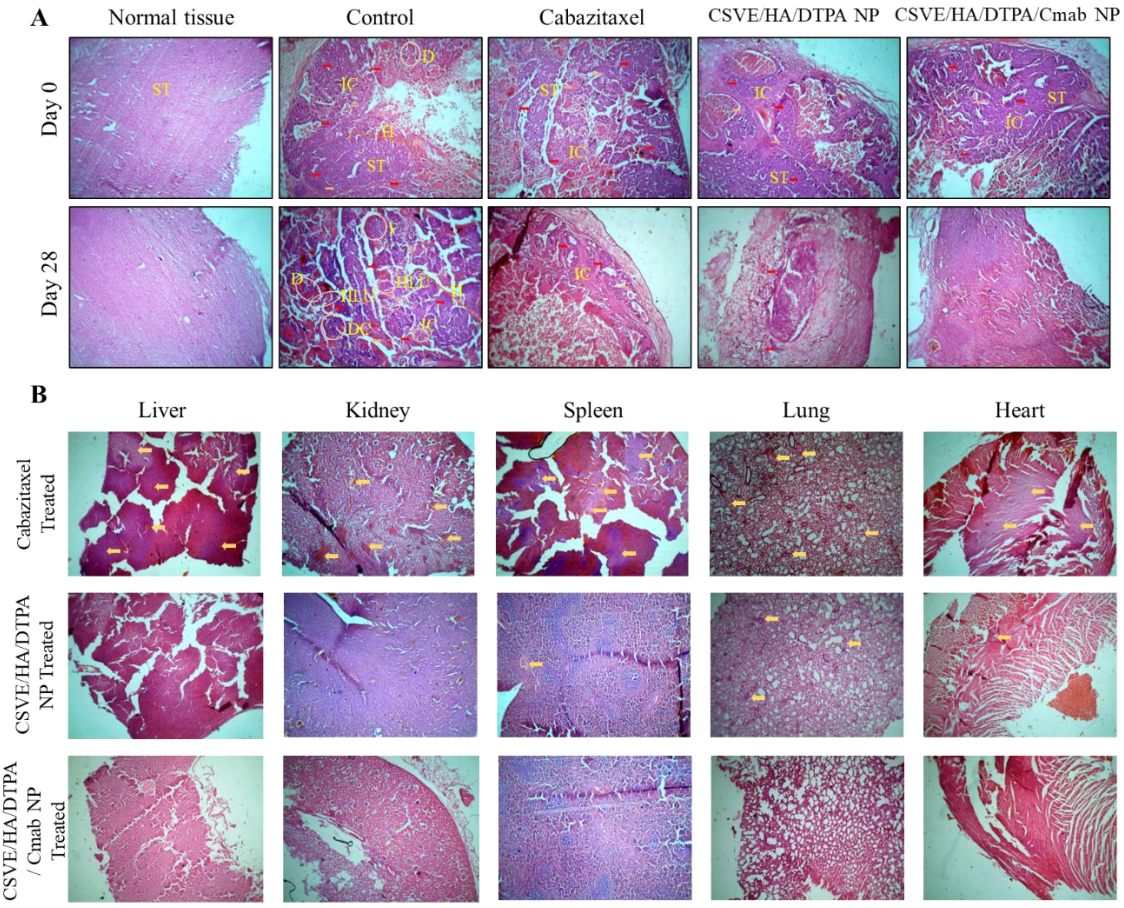

Figure 5.27 (A) Histological assessments of tumors isolated from rats after tumor regression study using H&E stain (magnification 4×; scale bar 100 µm) **(B)** Histological images of organ tissues after 28 days of treatment regimen. Invasive carcinoma (IC), stromal tissue (ST), proliferated and expanded terminal lobular units (HLU), dilated ducts

with inspissated secretions (D), Ductal Carcinoma (DC), Mucin (yellow arrow), Fibroadenoma (F) and breast hyperplasia (H).

The carcinoma had signs of increased proliferation and expansion of terminal lobular units (HLU), accompanied by expansion into surrounding fat tissue/adipocytes. The carcinoma showed dilated ducts with inspissated secretions (D), Ductal Carcinoma (DC), invasive cancer (IC), and Mucin (yellow arrow) [145]. The carcinoma also had presence of atrophy of glands with surrounding stromal fibrosis (Fibroadenoma, F) and breast hyperplasia (H) [144]. On treatment with CBT, although the breast hyperplasia area due to carcinoma decreased, but still had clear signs of cancer cells. Treatment with CSVE/HA/DTPA NP had effectively treated the breast cancer with only signs of remains of cancer cells. Although discontinuous membrane was still present in CSVE/HA/DTPA/Cmab NP treated groups, the carcinoma almost disappeared with complete disappearance of mucin and thick mass [143].

The histological investigation of all major organs including liver, kidney, spleen, lung and heart was also conducted to determine the safety of prepared formulation as compared to free cabazitaxel. Free cabazitaxel showed major signs of toxicity (yellow arrow, **Figure 5.27(B)**) in all major organs. In contrast, CSVE/HA/DTPA NP and CSVE/HA/DTPA/Cmab NP showed few or no signs of toxicity, suggesting the lower distribution of free drug from nanoparticles to all major organs. Therefore, prepared nanoformulation were safe and reduced the organ toxicity probably by minimizing the drug distribution to tissue and organs other than cancer.

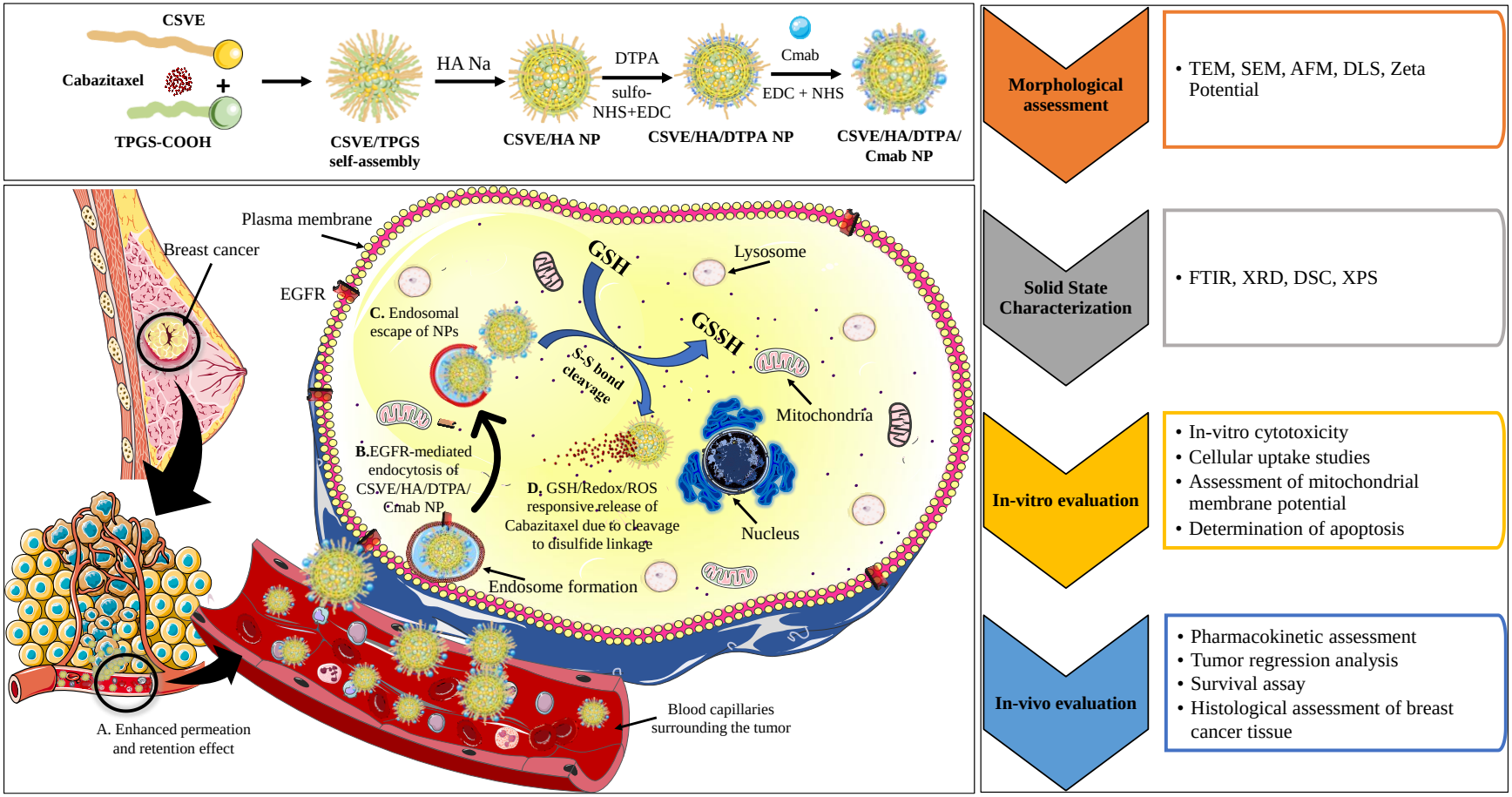

Figure 5.28 Graphical Summary of Objective 2